Eclogite and Garnet Pyroxenite Xenoliths from Kimberlites Emplaced Along the Southern Margin of the Kaapvaal Craton, Southern Africa: Mantle or Lower Crustal Fragments?

Anton Le Roex, Christel Tinguely, Michel Grégoire

Eclogite and garnet pyroxenite xenoliths from kimberlites emplaced along the southern margin of the Kaapvaal craton, southern Africa: mantle or lower crustal fragments?

Anton le Roex[1], Christel Tinguely[1] and Michel Gregoire[2]

[1]Department of Geological Sciences
University of Cape Town
Rondebosch, 7700
South Africa

[2]Geosciences Environment Toulouse
CNRS-CNES-IRD-Toulouse III University
Observatoire Midi-Pyrénées
31400 Toulouse
France

Corresponding author: Anton le Roex; +27-21-650-2926; anton.leroex@uct.ac.za

ABSTRACT

Eclogite xenoliths, together with garnet pyroxenites and some mafic garnet granulites, found in kimberlites located along the southern margin of the Kaapvaal craton in southern Africa have been analysed by electron microprobe and mass spectrometry techniques to determine their geochemical characteristics. The majority of eclogites are bimineralic with garnet and omphacitic clinopyroxene in subequal proportions, with rutile as the main accessory phase; a few contain kyanite. Based on K_2O in clinopyroxene and Na_2O in garnet, the eclogites can be classified as Group II eclogites, and the majority are high-Ca in character. Garnet pyroxenites comprise garnet clinopyroxenites and garnet websterites.

Major and trace element concentrations and isotope ratios of reconstituted bulk rock compositions of the eclogites and garnet pyroxenites allow constraints to be placed on depth of origin and likely protolith history. Calculated Fe-Mg exchange equilibration temperatures for the eclogites range from 815 to 1000 °C, at pressures of 1.7±0.4 GPa as determined by REE partitioning, indicating that they were sampled from depths of 50-55 km; i.e. within the lower crust of the Namaqua-Natal Belt. The garnet pyroxenites show slightly lower temperatures (686-835 °C) at similar pressures of equilibration. Initial $^{143}Nd/^{144}Nd$ and $^{87}Sr/^{86}Sr$ ratios (calculated to time of kimberlite emplacement) of both lithologies overlap the field for lower crustal samples from the Namaqua-Natal Belt. Further evidence for a crustal origin is found in the similar REE patterns shown by many of the associated garnet granulite xenoliths. Garnet pyroxenites are interpreted to have a similar origin as the associated eclogites but with the mafic protolith having insufficient Na (i.e. low modal plagioclase) to allow for development of omphacitic pyroxene. Metamorphism of the mafic protoliths to these eclogites and garnet pyroxenites is inferred to have occurred during crustal shortening and thickening associated with the collision of the Namaqua-Natal Belt with the Kaapvaal craton at 1-1.2 Ga.

Key words: eclogite; garnet pyroxenite; xenolith; geochemistry; petrogenesis

INTRODUCTION

Eclogite xenoliths hosted in kimberlite magmas are typically medium- to coarse-grained rocks comprising clinopyroxene and garnet in subequal proportions, plus a range of minor accessory phases including kyanite and rutile. By definition the clinopyroxene is omphacitic in composition,

and thus eclogites grade into garnet clinopyroxenites when the clinopyroxene is less Na-rich. Eclogites are a near ubiquitous lithology found within the xenolith suites of most kimberlite intrusions (e.g. Jacob, 2004) and at some localities on the Kaapvaal craton in southern Africa (e.g. Roberts Victor, Kaalvallei, Star, Orapa) they dominate the xenolith assemblage. As such, they clearly form an important component of the underlying lithospheric mantle (perhaps locally as much as 15%; Schulze, 1989), and provide insight into the composition, formation and evolutionary history of the continental lithosphere (Shirey *et al.*, 2001, Shirey *et al.*, 2002, Viljoen *et al.*, 2005, Viljoen *et al.*, 1996). Importantly, where shown to be mantle derived, they place constraints on craton root assembly and ancient continent stabilization (e.g. Jacob, 2004, Shirey *et al.*, 2001). Of importance in using eclogite xenoliths to infer their genesis and lithospheric evolution is that these rocks are extremely heterogeneous, as well illustrated by Hatton (1978) in his detailed study of the large (10 to >30 cm) eclogite xenoliths found in the on-craton Roberts Victor kimberlite. The near ubiquitous complex layering and banding found in the large Roberts Victor xenoliths suggests that small eclogite xenoliths (<few cm) are unlikely to be representative of the original mass of eclogite from which they were sampled, at least in terms of their modal mineral proportions. In interpreting the genesis of eclogite xenolith samples this complexity needs to be continually borne in mind.

Being largely bimineralic assemblages, early studies of mantle eclogite xenoliths were somewhat restricted in value. However, with the advent of microanalysis techniques such as SIMS and laser ablation ICP-MS, and improved isotope analysis of small samples, new insights have been gained on their formation and the nature of their protoliths (e.g. Appleyard *et al.*, 2007, Aulbach & Jacob, 2015, Aulbach *et al.*, 2017, Barth *et al.*, 2001, Barth *et al.*, 2002, Dludla *et al.*, 2006, Jacob, 2004, Jacob *et al.*, 2005, Kopylova *et al.*, 2016, Smit *et al.*, 2014, Viljoen, 1995, Viljoen *et al.*, 2005, Viljoen *et al.*, 1996). Subdivision of eclogite xenoliths into Group I and Group II varieties, primarily on textural (MacGregor & Carter, 1970) and specifically chemical variations (McCandless & Gurney, 1989), is well established. Most relatively recent studies of eclogites hosted by on-craton kimberlites argue that they (particularly Group I eclogites) represent variably modified recycled Archean mafic oceanic crust, tectonically attached/emplaced into the subcontinental lithosphere during subduction (e.g. Aulbach *et al.*, 2016, Aulbach & Jacob, 2015, Aulbach & Jacob, 2016, Aulbach *et al.*, 2017, Barth *et al.*, 2001, Barth *et al.*, 2002, Jacob *et al.*, 1994, Jacob, 2004, Jacob *et al.*, 2005, Viljoen *et al.*, 2005). Less commonly (e.g. Barth *et al.*, 2001, Ireland *et al.*, 1994, Rollinson, 1997, Snyder *et al.*, 1997) it has been argued that some eclogites are restites of Archean granitoid crust formation and tonalitic melt extraction processes,

which have subsequently foundered into the underlying upper mantle. Such models align with combined petrological and geophysical evidence from eastern Australia for an imbricated continental crust-mantle boundary of layered granulite/eclogite and peridotite (Griffin & O'Reilly, 1986, Pearson *et al.*, 1991). In addition to the Group I versus Group II subdivision, low-MgO and high-MgO eclogites are recognised, with the latter argued to result from the interaction of a siliceous melt derived from the down-going slab with the overlying peridotite mantle (e.g. Snyder *et al.*, 1997, Taylor *et al.*, 2003).

Very much less attention has been paid to eclogite xenolith suites from circum- and off-craton regions, and in southern Africa the only modern detailed study has been on the eclogite xenoliths from the Rietfontein kimberlite (Appleyard *et al.*, 2007) located in the Proterozoic Rehoboth subprovince to the west of the Kaapvaal craton. The cluster of Cretaceous age kimberlites emplaced along the southern margin and adjacent off-craton region within the Proterozoic Namaqua-Natal Belt have xenolith assemblages that include both peridotitic varieties (lherzolite, garnet lherzolite) and eclogitic, pyroxenitic and granulitic varieties (Robey, 1981). The latter lithologies are found particularly in the Goedehoop, Jachtfontein, Lovedale, Markt and Roodekraal kimberlites and form the basis of this study. Tinguely *et al.* (2008) have provided initial descriptions of the rocks reported on here. Focus in this study is on the eclogites *senso stricto* and garnet pyroxenites (clinopyroxenites and websterites) from these five craton margin locations, with some comparisons drawn from the associated garnet granulites.

GEOLOGICAL SETTING AND SAMPLING

The Kaapvaal craton in southern Africa is surrounded by several major Proterozoic terranes: the Kheis Province to the west; the Limpopo Belt to the north; and the Namaqua-Natal Belt to the south and southeast (Fig. 1). The eclogites that are the focus of this study were recovered from Cretaceous kimberlites occurring in the vicinity of Britstown (Goedehoop, Jachtfontein, Lovedale, Roodekraal) and to the northwest (Markt), along the southern margin of the Kaapvaal craton (Fig. 1). Whereas the exact location of the southern boundary to the craton is poorly constrained, it is commonly considered to be the Brakbos fault in the southwest and its inferred extension below the Karoo surface rocks to the southeast (e.g. Schmitz & Bowring, 2004). Accepting that the boundary is represented by the Brakbos fault, then Markt is clearly off-craton, within the southern extension of the Gordonia subprovince of the Namaqua-Natal Belt, whereas the Goedehoop, Jachtfontein, Lovedale, and Roodekraal localities are somewhat ambiguous in terms of their position relative to

the craton margin. The host kimberlites have been reported on by Robey (1981), Harris *et al.* (2004) and Becker and le Roex (2006). In addition to eclogite, the kimberlites have brought to the surface as xenolithic fragments a range of mantle peridotites and deep crustal rocks such as amphibolite, granulite and garnet granulite (Robey, 1981). Peridotitic xenoliths from this cluster of kimberlites have been described in le Roex and Class (2016) and Robey (1981), whereas the granulitic xenoliths from the Namaqua-Natal Belt in general have been reported on by Robey (1981), Pearson *et al.* (1995), Huang *et al.* (1995), Schmitz and Bowring (2004) and Long (2005).

The Namaqua-Natal Belt comprises a wide variety of rock types, ranging from approximately 2 Ga low- to medium-grade supracrustal rocks (Richtersveld Subprovince), and 2 Ga granite gneisses and medium- to high-grade 1.6-1.2 Ga amphibolite to granulite grade supracrustal rocks, together with syn- and post-tectonic intrusive granitoids of the Bushmanland Terrane (Cornell *et al.*, 2006). Terranes to the west (Richtersveld and Bushmanland) have been interpreted to reflect a Paleoproterozoic microcontinent (comprising multiple accreted volcanic arcs; Cornell *et al.*, 2006, Schmitz & Bowring, 2004) that was accreted to the southwestern margin of the Kaapvaal Craton at 1.3-1.0 Ga (Schmitz & Bowring, 2004). The Natal Terrane to the east is thought to be a former continental margin that was deformed during its collision with the Kaapvaal Craton at a similar time (Schmitz & Bowring, 2004). The Namaqua-Natal Orogeny at about 1.1 Ga led to major SW-NE crustal shortening across the entire Namaqua-Natal Province (Cornell *et al.*, 2006). The overall crustal thickness in the region of interest, and through which the kimberlites were likely emplaced, is estimated from seismic studies to be 45-50 km (Nguuri *et al.*, 2001) due to collisional foreshortening of the crust and magmatic emplacement, in contrast to the ~35-40 km crustal thickness of the southern Kaapvaal Craton (Levander *et al.*, 2006). Undeformed sedimentary and intrusive rocks of the Karoo Super Group overly the metamorphic rocks of the Namaqua-Natal Belt in the region of interest. The presence of Archaean (~2.6 Ga) zircon in a single eclogite xenolith from the Lovedale kimberlite described by Schmitz and Bowring (2000) raises the question as to whether the Lovedale kimberlite rose through and sampled the Archaean Kaapvaal crust, or whether Archaean fragments exist in the otherwise early Proterozoic terrain that collided with the Kaapvaal craton during the Namaqua-Natal orogeny (Schmitz & Bowring, 2004).

Eclogite xenoliths are described from three kimberlite pipes exposed in the Britstown area: Jachtfontein (31°00'S 24°15'E), Lovedale (30°34'S 23°35'E) emplaced at ~74 Ma (Smith *et al.*, 1994) and Roodekraal (30°48'S 24°13'E); and from Markt a little to the northwest (30°15'S 22°21'E) and emplaced at ~116 Ma (Smith *et al.*, 1994). In addition, garnet pyroxenite xenoliths

were analysed from Jachtfontein, Roodekraal, Markt and the Goedehoop kimberlite (30°50'S, 24°24'E) emplaced at 74.4 Ma (Smith *et al.*, 1994). Although not a major focus of this study, a few garnet granulites from Goedehoop, Jachtfontein, Lovedale and Roodekraal were analysed for comparative purposes. Some of the eclogite, garnet pyroxenite and garnet granulite samples from Jachtfontein, Lovedale and Markt were collected in the field by the authors, the remainder from these localities, and those from Roodekraal, were obtained from the 'Mantle Room' collection housed at the University of Cape Town. In describing samples in this study, we distinguished between eclogite *senso stricto* and garnet clinopyroxenite in the former having jadeite contents of clinopyroxene greater than 15% and diopside less than 80%, with garnet plus clinopyroxene making up more than 75% of the rock. Garnet websterites were classified based on having >10% orthopyroxene in addition to clinopyroxene and garnet.

ANALYTICAL

Constituent minerals of the samples were analysed by a range of analytical techniques to determine their major element, trace element, radiogenic isotope and stable isotope compositions.

Major elements

Major element analyses were performed on 60μm thick polished sections using a Cameca SX50 electron microprobe at the Observatoire Midi-Pyrénées (Toulouse, France), at an accelerating voltage of 15kV and a beam current of 20 nA. Counting times were 10 sec on the peak and 2 x 5 sec on the background for all elements except Na and K for which the counting times were 30 sec and 2 x 15 sec on peak and background, respectively. Natural and synthetic standards were used and the matrix corrections were performed using the method of Pouchou and Pichoir (1984). Further details of the operating conditions, errors and detection limits can be found in le Roex and Class (2016).

Trace elements

Twenty-five trace element concentrations in constituent minerals were determined by laser ablation ICP-MS on 100 μm polished sections using quadrupole Perkin-Elmer ELAN6000 ICP-MS instruments coupled to Cetac LSX-200 laser ablation modules at the University of Cape Town and at Observatoire Midi-Pyrénées (Toulouse, France). The repetition rate of the 266 nm frequency-quadrupled Nd-YAG laser was set between 5-10 Hz and depending on the grain size of the mineral analysed, the beam diameter was set at 62.5, 100 or 200 μm. A 30 second read delay was conducted before each analysis. The main gas flow was set at 15 $l.min^{-1}$, the auxiliary gas

flow at 0.75 l.min^{-1}, and the nebuliser gas flow at ~1.06 l.min^{-1}. A typical analysis consisted of 3 replicates of 50-100 readings each, and normalisation of the data was achieved using internal standards (^{43}Ca, ^{25}Mg or ^{27}Al – Toulouse; ^{29}Si – Cape Town). Concentrations were calibrated against NIST610 and NIST612 glass reference materials (Norman *et al.*, 1996, Pearce *et al.*, 1997). A double normalisation approach (Longerich *et al.*, 1996) was used to correct for instrumental drift. Detection limits calculated on the gas blank range from 10–20 ppb for REE, Ba, Rb, Th, U, Nb, Ta, Pb, Sr, Zr, Hf, Y to 100 ppb for V, Sc and to 2 ppm for Ti, Ni and Cr. Typical precision and accuracy range from 1 to 10% for concentrations above 1 ppm, and deteriorates as expected at lower concentrations. Analyses of international rock reference standards undertaken at the same time, illustrating typical accuracy and precision over a range of concentrations, are reported in le Roux *et al.* (2002).

Stable isotopes

$\delta^{18}O$ values ($^{18}O/^{16}O$ expressed in parts per thousand – permil – relative to that of VSMOW) were determined on hand-picked garnet and clinopyroxene from selected eclogites at the Institute of Mineralogy and Geochemistry (University of Lausanne) and Department of Geological Sciences (Cape Town). After washing in an ultrasonic bath with Decon (5 min), milliQ (5 min) and 15% HF (10 min) one to three mineral grains, weighing between 1 and 2 mg, were loaded into a 12 sample platinum block with 2 quartz and 2 garnet standards (Lausanne), or with 2 garnet standards (Cape Town). Analytical procedures were identical at both laboratories, the only difference being that samples were reacted with fluorine in Lausanne and with BrF_5 in Cape Town. Correction of the data in Lausanne was against NBS-28 ($\delta^{18}O_{norm} = \delta^{18}O_{raw} - |\delta^{18}O_{NBS28}-9.64|$), whereas in Cape Town it was against Monastery garnet ($\delta^{18}O_{norm} = \delta^{18}O_{raw} - |\delta^{18}O_{MON}-5.39|$). Repeat analyses within laboratories and between laboratories have 2σ values ranging from 0.08 to 0.72 (determined by two to three repeat analyses of each of six garnets and four clinopyroxenes). Replicate (n=9) measurements of internal garnet standards UWG2 (Lausanne) and Monastery garnet (UCT), and international quartz standard NBS28 gave the following results: NBS28 = 9.63‰±0.28 (accepted value 9.64‰); UWG2 = 5.51‰±0.93 (accepted value = 5.8‰); Monastery garnet = 5.34‰±0.32 (accepted value = 5.55‰). Further details can be found in Harris and Vogeli (2010).

Radiogenic isotopes

Sr, Nd and Pb isotopes were determined on clinopyroxene from selected samples using a NuPlasma Multi-collector ICP-MS at the University of Cape Town. Nd and Pb were determined on solutions whereas Sr isotopes were determined by laser ablation, with a subset on solutions.

Pb isotopes were separated from the matrix by conventional dissolution and ion chromatography procedures and the final extract then diluted to ~50 ppb Pb solution using 2% HNO_3 doped with 100 ppb Thallium. Blanks were measured for 30 seconds on the same acids used for dissolution, and then the sample analysis typically comprised 3 blocks of 20 measurements each (each measurement taking 10 seconds). Instrumental drift was corrected for by normalising against the SRM981/997 reference standard (accepted values: $^{208}Pb/^{204}Pb = 36.7219 \pm 0.0044$ (2σ); $^{207}Pb/^{204}Pb = 15.4963 \pm 0.0016$ (2σ); $^{206}Pb/^{204}Pb = 16.9405 \pm 0.0015$ (2σ); (Galer & Abouchami, 1998) which was analysed before the first sample and then after every four to five samples. Over two days the 9 measurements of the SRM981/997 reference standard yielded an average of $^{208}Pb/^{204}Pb = 36.7314 \pm 0.0187$ (2σ); $^{207}Pb/^{204}Pb = 15.5021 \pm 0.0064$ (2σ); $^{206}Pb/^{204}Pb = 16.9466 \pm 0.0057$ (2σ). More details of the technique and associated errors are reported in Harris *et al.* (2015).

Nd isotopes were measured on clinopyroxene from selected samples using conventional dissolution and ion chromatography methods. The final Nd extract was diluted in 2% HNO_3 to a concentration level of ~50 ppb. The analytical procedure was the same as for Pb isotopes, although the blank was determined for each sample by ESA deflection for 30 seconds. A 50 ppb solution of the Nd reference standard JNdi-1 (accepted value =0.512115; Tanaka *et al.*, 2000) was used for standard bracketing. Over two days, the 11 measurements of JNdi-1 yielded an average value of 0.512068 ± 0.000021 (2σ). More details of the technique and associated errors are reported in Harris *et al.* (2015).

Sr isotopes were determined using laser ablation techniques and solution analysis. Solution analysis followed conventional dissolution and ion chromatography methods and the final Sr extract was then diluted in 2% HNO3 to 150 to 200 ppb Sr. The analytical procedure was similar to that described for Pb; background measurement was done on the acid blank and the sample analyses bracketed by analysing the SRM987 reference standard (accepted value = 0.71025). The average ratio for the bracketing measurements using SRM987 was 0.71028 ± 0.00002 (2σ). More details of the technique and associated errors are reported in Harris *et al.* (2015).

Sr isotopes measured by laser ablation ICP-MS made use of a New Wave 213 nm Nd-YAG laser coupled to the NuPlasma Multi-collector ICP-MS at the University of Cape Town, as described in detail in Copeland *et al.* (2008). The ablation sample cell was flushed using He (~0.4 l /min), with Ar (0.70 l/min) mixed into the line prior to arrival at the plasma. Sr isotopes were measured using static multi-collection using 12 Faradays. Analyses were made using line scans with preablation followed by a purge of 90 seconds, a 30 second measurement of the gas blank (to monitor ^{86}Kr), and 200 seconds of ablation along the pre-ablated line. Spot size for the analyses was set to 200 μm, speed was 5 μm/s at 90% power and with a repetition rate of 20 Hz. Measured isotope ratios were corrected for instrument fractionation using the exponential law and a $^{86}Sr/^{88}Sr$ ratio of 0.1194. The interference of ^{87}Rb on ^{87}Sr was corrected using the ^{85}Rb ion signal. The correction is considered good for voltages of ^{85}Rb that are less than 0.30% of the total Sr voltage. In all cases this value was less than 0.10%. The in-house clinopyroxene standard JJG1424 (from a garnet websterite) was used for bracketing using the accepted value of 0.70495. Repeat measurements of JJG1424 during the course of this study yielded an average $^{87}Sr/^{86}Sr$ 0.70490 ± 0.0006 (n=112). With one exception (garnet websterite 20770), the nine samples where Sr was determined by both solution and laser analyses show an excellent correlation (r^2=0.99 excluding sample 20770), with the laser analyses being within error of the solution analyses (Electronic Appendix 1; http://www.petrology.oxfordjournals.org).

PETROGRAPHY

Most samples were small (many only a few centimetres in diameter) and some were available only as polished-sections. Given the coarse grain size (typically >1-2 mm) and banding that is sometimes present, modal proportions estimated in thin-sections are unlikely to represent the bulk rock. Nevertheless, estimates of garnet, clinopyroxene and accessory phases were made based on 1000 point-counts on a polished section. Important accessory phases such as rutile are highly scattered in their distribution and estimated proportions are even more unlikely to be accurate with respect to the bulk rock. A summary of main petrographic features of the eclogite and garnet pyroxenite samples is provided in Table 1 and elaborated on below; textures of selected eclogite samples are shown in Fig. 2. The main petrographic features of the analysed garnet granulites are summarised below and in Electronic Appendix 2.

Eclogites

Twenty-nine bimineralic eclogites and three kyanite eclogites have been studied (Table 1) from the four craton margin kimberlite localities. One sample (20720 from Jachtfontein) is composite in having half the thin-section comprising eclogite (20720e) and the other half garnet granulite (20720g; Fig. 2b). The eclogites are medium to coarse grained with textures ranging from granoblastic to mosaic granoblastic with eight samples showing distinct banding of clinopyroxene and garnet (20163; 20263; 20700; 02100; 026203I; 026203J; 42153, 42223). Clinopyroxene and garnet range in modal abundance from ~40 to ~60 vol.% with both minerals showing sub-rounded to sub-angular habits. Garnets tend to be slightly smaller than associated clinopyroxene, and kelyphite rims are common. Subrounded to subhedral grains of rutile (2-3 vol.%) occur as an accessory phase in nearly all samples; where absent thin-section heterogeneity might be the cause. Phlogopite (< 2 vol.%) occurs as a secondary interstitial phase in fractures and along grain boundaries and sanidine (~5 vol.%) occurs as "pools" in two samples from Markt – 10063 and JJG2294.

The kyanite eclogites are similar in their petrography to the bimineralic eclogites, differing only in the presence of kyanite (3 to 7 vol.%) which occurs as elongated laths 0.5 to 3 mm in length (Fig. 2). All are coarse-grained and textures are granoblastic.

Garnet clinopyroxenites

The five garnet clinopyroxenites analysed are medium to coarse grained with granoblastic to mosaic granoblastic textures (Table 1). Clinopyroxene and garnet have irregular through subrounded to subhedral habits, and range in modal abundance from 48 to 64 and 34 to 49 vol.%, respectively. Triple point junctions are common. Garnets are characterised by having thick kelyphite rims and clinopyroxenes commonly show fine exsolution of orthopyroxene. Rutile (1 to 2 vol.%) is the main accessory mineral, occurring as fine, sub-rounded to subangular interstitial grains, but it may also occur as fine inclusions in clinopyroxene and garnet. Secondary phlogopite is ubiquitous in all samples, occurring as anhedral grains in fractures and along grain boundaries.

Garnet websterites

The five garnet websterites analysed are coarse to medium grained with granoblastic to mosaic granoblastic textures. A summary of their petrographic characteristics is provided in Table 1. Clinopyroxene (41 to 66 vol.%), garnet (17 to 30 vol.%) and orthopyroxene (10-37 vol.%) have subrounded to subhedral habits. Some orthopyroxenes contain subrounded inclusions of garnet. Accessory phases include rutile, spinel and ilmenite. Kelyphite as an alteration product around

garnets is ubiquitous in all samples. Anhedral phlogopite is the main secondary phase and occurs in cross-cutting fractures and along some grain boundaries.

Garnet granulites

Garnet granulites are a common lithology amongst the xenolith population of these craton margin kimberlites. Although not a focus of this study, a total of 16 garnet granulites were studied for comparative purposes, one of which (20720g) from Jachtfontein shares a contact with eclogite sample 20720e.

Samples range from fine- to coarse-grained and most samples exhibit granoblastic textures, with common mineral banding. Straight grain boundaries and 120^{o} triple junctions are ubiquitous. Three samples (42303, GHP01, GHP05) exhibit a mosaic granoblastic texture. Clinopyroxene ranges in modal abundance from 20 to 49 vol.% and is subrounded to subangular in shape. Subrounded inclusions of garnet and plagioclase may occur within clinopyroxene. Garnet ranges in modal abundance from 20 to 37 vol.% abundance, is mostly subangular but may occur as poikiloblastic grains. Subrounded inclusions of clinopyroxene are frequent, and in one sample (02GG11) inclusions of plagioclase occur within garnet. Coronas of kelyphitic material around the garnets are common. Plagioclase ranges in modal abundance from 20 to 48 vol.% and often exhibits inclusions of clinopyroxene. Rutile occurs in most samples (1-3 vol%), mostly as scattered grains but may also occur as inclusions within clinopyroxene, garnet or plagioclase. In a number of samples mica occurs as a secondary accessory phase along grain boundaries or within fractures. A summary of the petrographic characteristics of these samples is provided in Electronic Appendix 2 and mineral analyses are reported in Electronic Appendix 3.

MINERAL CHEMISTRY

Eclogites

Mineral major element compositions and end-member components are reported in Table 2 and illustrated in Figs. 3 and 4. Garnet compositions vary widely, with Mg# (atomic Mg/(Mg + Fe)) ranging from 0.36 to 0.69 and Ca# (atomic Ca/(Mg + Fe + Mn + Ca)) from 0.11 to 0.32 (Fig. 3a). In contrast, clinopyroxene compositions range in Mg# from 0.66 to 0.91 and are omphacitic in character, with greater than 13% jadeite component (Fig.4; Table 2). Garnets plot largely within the field for southern African on-craton eclogitic garnets on a Ca# - Mg# plot (Fig. 3a), and using the terminology of Aulbach *et al.* (2017) the majority of samples can be classified as High-Ca

eclogites. A few garnets plot within the Low-Mg eclogite field and a single sample (42233) from Roodekraal plots in the field of High-Mg eclogites (Fig. 3a). Clinopyroxenes have 5.4 to 13.1 wt% Al_2O_3, 0.07 to 0.45 wt% TiO_2 and 3.1 to 7.0 wt% Na_2O, whereas garnets have <0.15 wt% TiO_2, <0.4 wt% Cr_2O_3 and <0.09 wt% Na_2O. CaO in garnets ranges from 4.2 to 12.1 wt%, and FeO* and MgO range from 11.6 to 25.6 wt.% and from 7.3 to 16.2 wt%, respectively (Table 2). The low Na_2O (<0.09 wt%) content of the garnets (bar three – 02083, 026203I, 026203J) and low K_2O (<0.02 wt%) content of the clinopyroxenes suggest that they are best classified using the McCandless and Gurney (1989) approach as Group II eclogites (Fig. 3b). In terms of Na_2O-MgO variation in clinopyroxene (Fig. 4b), the eclogites fall largely within the Group B field of Taylor and Neal (1989).

Trace element and rare earth element abundances in clinopyroxenes and garnets are quite varied (Table 2). High field strength (Zr excepted) and large ion lithophile elements (Rb, Ba, U) are generally low to extremely low in both minerals (<<1 ppm), although Rb and Ba do reach high concentrations in a few samples (Rb up to 14 ppm and Ba up to 380 ppm in clinopyroxene; Table 2). These high values are interpreted to reflect a contribution from subsurface fractures contaminated by host kimberlite or low temperature alteration effects. The data are reported in Table 2 for completeness but since they are not primary characteristics they are not used in subsequent interpretations or calculations. Other trace elements in these samples do not appear to have been affected. In clinopyroxene, Sr (2-880 ppm), Zr (1-76 ppm), Sc (3-53 ppm), Cr (55-850 ppm), V (26-645 ppm) and Ni (12-549 ppm) are variable, extending to high concentrations. Light rare earth elements (LREE) reach relatively high concentrations (La up to 19 ppm and Nd up to 70 ppm), whereas the heavy rare earth elements (HREE) extend to very low concentrations (Yb less than 0.27 ppm). Chondrite normalised REE abundances in clinopyroxene describe smooth patterns ranging from flat to strongly LREE enriched (La/Sm_n =3.5; La/Yb_n =144); some show a significant (positive or negative) Eu anomaly (Eu/Eu*=0.7-2.3; where Eu*=interpolated chondrite normalised value between Sm and Gd [$=Sm^{1/2} \times Gd^{1/2}$]). Representative REE patterns are shown in Fig. 5.

Garnets have variable, extending to high, concentrations of Zr (1.5-48.5 ppm), Sc (33-119 ppm), V (14.5-256 ppm) and Ni (3-53 ppm). LREE are strongly depleted (La less than 0.3 ppm) and HREE are enriched (Yb up to 6 ppm), with chondrite normalised patterns consequently showing strong LREE depletion with high and largely constant HREE (La/Sm_n=0.17; Gd/Yb_n=1.7). Like

clinopyroxene, some garnets show positive Eu anomalies of similar magnitude. Representative chondrite normalised REE plots of the garnets are shown in Fig. 5.

Garnet clinopyroxenites and garnet websterites

Clinopyroxenes in the garnet clinopyroxenites and websterites are Cr-poor diopsides, in contrast to the omphacites in the eclogites, and extend to slightly more Mg-rich compositions (Table 3; Fig. 4a). They have <0.47 wt.% Cr_2O_3, 0.82 to 6.1 wt.% Al_2O_3, <0.23 wt.% TiO_2, and <2.7 wt.% Na_2O (42103 excepted with 4.1 wt.% Na_2O). Mg#s range from 0.75 to 0.95. There is no systematic difference in composition between the clinopyroxenes in the clinopyroxenites and websterites. Orthopyroxenes in the garnet websterites are Mg-rich (Mg# = 0.74 to 0.91) and have <0.35 wt.% Cr_2O_3, <1.6 wt.% Al_2O_3 and <0.27 wt.% CaO (Table 3). Garnets are pyrope-almandine in composition and Mg#s vary widely (0.44-0.74), extending to slightly more Mg-rich compositions than garnets in the eclogites (Table 3; Fig. 4a). MgO and FeO* contents vary from 10.1 to 16.1 wt.% and from 12.5 to 23.5 wt.%, respectively. They have <0.1 wt.% TiO_2, <1.9 wt.% Cr_2O_3 and <0.1 wt.% Na_2O. Garnets in the websterites have Cr_2O_3 contents which are slightly higher and more variable (0.88±0.8 wt.%) than those in the clinopyroxenites (0.15±0.08 wt.%).

Trace element and rare earth element abundances in clinopyroxenes and garnets in the garnet pyroxenites are quite variable (Table 3). In clinopyroxene, Sr (20-350 ppm), Zr (1.5-94 ppm), Sc (12-72 ppm), V (114-507 ppm) and Ni (118-585 ppm) extend to high concentrations and overlap with those in the eclogite clinopyroxenes. Large ion lithophile elements (Rb, Ba, U), Th, Nb and Ta are generally low to extremely low in both minerals (<<1 ppm). The elevated Ba (and Rb) in samples RDK-1 (cpx) and 20043 (gt) are attributed to kimberlite contamination or alteration effects and are not used in subsequent interpretations or calculations. Chondrite normalised REE patterns show strong relative depletion in the HREE (Yb_n<0.6), with strong enrichment in middle and light REE which show a convex upward pattern (Electronic Appendix 4). Clinopyroxenes in two garnet websterites (20063 and 20770 from Jachtfontein) do not show the characteristic convex-up middle and light REE enrichment and show an overall flatter enrichment pattern (Electronic Appendix 4).

Garnets have variable, extending to high concentrations of Zr (3.2-31.4 ppm), Sc (58.4-208 ppm), V (48-273 ppm) and Ni (4.9-14 ppm). LREE are strongly depleted (La less than 0.4 x chondrite) and HREE are enriched (Yb >10 x chondrite), with chondrite normalised REE patterns (Electronic

Appendix 4) consequently showing strong LREE depletion (La/Sm_n<0.09) with high and largely constant HREE (Gd/Yb_n=0.3-3.3). A number of garnets show an unusual upturn in the pattern at La (and sometimes Ce). This could reflect analytical error on the very low concentrations (La<0.08 ppm), or reflect the early stages of cryptic metasomatism, as shown in the associated off-craton peridotites (le Roex & Class, 2016). It is notable that neither the clinopyroxenes nor the garnets from the garnet pyroxenites show evidence of any Eu anomaly.

RADIOGENIC AND STABLE ISOTOPES

Sr, Nd and Pb isotope ratios in clinopyroxene and O-isotope ratios in clinopyroxene and garnet were determined in a subset of samples and are reported in Table 4. Due to the size of the samples and degree of weathering, not all isotope systems could be determined on all samples. Initial $^{87}Sr/^{86}Sr$ values for clinopyroxenes in the eclogites (calculated to the age of the host kimberlite) range from 0.70350 to 0.70707 and $^{143}Nd/^{144}Nd$ values range from 0.51129 to 0.51266. The clinopyroxenes from the pyroxenites show a similar range with $^{87}Sr/^{86}Sr$ =0.70254 to 0.70619 and $^{143}Nd/^{144}Nd$ =0.51129 to 0.51263. Fig. 6a shows a plot of $^{87}Sr/^{86}Sr_i$ versus $^{143}Nd/^{144}Nd_i$ where it is clear that clinopyroxenes from most samples plot below the mantle array, with those from two eclogite samples, 42123 and 42143, both from Roodekraal, plotting within the depleted quadrant close to the mantle array. Clinopyroxene from garnet websterite 20770 from Jachtfontein similarly plots just within the depleted quadrant. Roodekraal and Jachtfontein kimberlites are Group I off-craton kimberlites (Robey, 1981) and although isotope data are not available for these specific kimberlites, the samples from both localities plot close to the field of South African Group I kimberlites (Fig. 6a) and contamination by the host kimberlite cannot be discounted. *[Note: where samples do not have corresponding Nd data (for example, laser ablation Sr determinations) the data points are arbitrarily plotted on the base-line ($^{143}Nd/^{144}Nd_i$ = 0.5112) to illustrate the spread in Sr isotope ratios].* Clinopyroxenes show a strong positive correlation between $^{143}Nd/^{144}Nd$ and Sm/Nd ratio, indicating reasonably closed- system radiogenic in-growth. Pb isotopes are equally variable ($^{206}Pb/^{204}Pb$=17.26-19.45; $^{207}Pb/^{204}Pb$=15.53-15.59; $^{208}Pb/^{204}Pb$=37.1-41.93). Sample 42233 from Roodekraal has exceptionally high $^{208}Pb/^{204}Pb$ (41.9) relative to its $^{206}Pb/^{204}Pb$ ratio of 19.45 and the Northern Hemisphere Reference Line (Hart, 1984; not shown).

Measured oxygen isotope compositions in clinopyroxene and garnet from eclogite samples range in $\delta^{18}O$ from values typical of the upper mantle (5.1‰) to higher values (7.5‰). The latter value is from a clinopyroxene and so might not be as robust (due to alteration of the clinopyroxene) as that from the coexisting garnet which gives a $\delta^{18}O$ value of 6.8‰. The range in $\delta^{18}O$ from 5.1 to 6.8‰

falls well within the range of published data for eclogites from various cratonic regions (Fig. 6c) and overlaps with that determined from eclogites from the South African off-craton Rietfontein locality (Appleyard *et al.*, 2007). The garnet clinopyroxenites and websterites show a similar range in $\delta^{18}O$ (~5 to ~7‰) to that shown by the craton margin eclogites (Table 4; Fig. 6c).

BULK ROCK COMPOSITIONS

The small sizes of the eclogite xenoliths and likely contamination along fractures and grain boundaries by the host kimberlite magma makes the value of analysis of whole rock samples questionable. Consequently, we have reconstructed the bulk rock compositions from constituent mineral compositions combined with their modal abundances, as is common practice in eclogite studies (e.g. Barth *et al.*, 2001, Jacob, 2004). Modal abundances in the eclogites range from 58 vol% to 35 vol% garnet and 62 vol% to 39 vol% clinopyroxene. Given the relatively large grain size and presence of banding in many samples, an average of 50% garnet and 50% clinopyroxene has been used in the calculations, modified for minor rutile or kyanite (see below). It is not as easy to calculate bulk rock compositions for the pyroxenites as the modal abundances of garnet, clinopyroxene and, in the case of the websterites, orthopyroxene are more variable, and less constrained. In the case of the garnet pyroxenites, estimated modal abundances based on point counting have therefore been used in the calculation of bulk rock composition. Since the orthopyroxenes have not been analysed for their trace element content, and with the exception of the transition metals, generally would have very low trace element abundances (e.g. Rehfeldt *et al.*, 2008), the bulk rock trace element compositions of the garnet websterites have been calculated assuming that orthopyroxene acts as a dilutant; concentrations of transition metals have not been calculated.

The primary accessory phase is rutile (<3 vol.%), and although not present in all sections, where absent it may simply reflect its inhomogeneous distribution at the thin-section scale. Kyanite is the second most important accessory phase occurring only in three samples and its estimated modal abundance has been used in the calculation for these samples. The primary impact that rutile has on the bulk composition, other than on Ti, is on Nb and Ta, and to a lesser extent Zr and Hf. The bulk rock Ti concentrations have been determined using the same approach as that used by Aulbach and Jacob (2016). The amount of rutile nominally in the eclogite has been determined by assuming that there should be no negative Ti anomaly on a primitive mantle normalised diagram (since MORB, the commonly inferred precursor to many mantle eclogites, does not show a negative Ti anomaly). The bulk rock Ti abundances reported in Table 5 have been adjusted to

reflect the amount of rutile calculated for each sample using this approach. In the absence of laser ablation data for Nb, Ta, Za and Hf in rutile in these samples the reported Nb and Ta, and to a lesser extent Zr and Hf, abundances in Table 5 are thus underestimates.

Figure 7 shows the variation of selected major elements in the reconstructed bulk rock eclogite and garnet pyroxenite compositions (values provided in Table 5 and Electronic Appendix 5). As would be expected, bulk compositions are "basaltic" in nature. Compared to eclogites from the Kaapvaal craton (Fig. 7), these craton margin eclogites show more allegiance to Group I compositions than to Group II compositions, but extend to lower Mg# (0.80-0.51; Fe_2O_3/FeO=0.15), have slightly lower SiO_2 (45.9-48.3 wt%), FeO* (6.9-16.8 wt%) and MgO (6.9-14.6 wt%), and higher CaO (9.6-15.3 wt%). Al_2O_3 (13.8-18.3 wt%) abundances are similar to those of Kaapvaal craton Group I eclogites. Two of the three kyanite eclogites show elevated Al_2O_3 (17.5 to 20.6 wt%), but otherwise show no systematic differences from the bimineralic eclogites in their major element compositions, unlike those from the Rietfontein kimberlite (Appleyard *et al.*, 2007) which have lower Mg# and higher Al_2O_3 than their bimineralic equivalents (Fig. 7). The garnet pyroxenites and particularly the garnet websterites tend to be more SiO_2-rich than the craton margin eclogites, with the websterites having significantly lower Al_2O_3 concentrations (4.5-7.7 wt.%). The garnet pyroxenites extend to more Mg-rich compositions (Mg# ~0.90) and are significantly more MgO-rich (MgO=12-20 wt.%) at a given FeO content than the eclogites (Fig. 7).

Reconstructed bulk rock trace element abundances are highly variable (Table 5; Electronic Appendix 5) and variations in selected elements are depicted in Fig. 8. Transition metals in the eclogites are high and variable (Ni=8-296 ppm; Cr=100-850 ppm; Sc=20-69 ppm), and the more immobile incompatible elements are highly variable (Sr=5-444 ppm; Zr=1-78 ppm; Th=0.015-0.68 ppm; La=0.07-6.0 ppm; Ce=0.07-24.2 ppm). The mobile incompatible elements are mostly very low in abundance as would be expected but extend to high values in a few eclogite samples: Rb=0.005-13 ppm; Ba=0.02-190 ppm; U=0.012-0.405 ppm (Table 5). The light rare earth elements tend to show excellent correlations amongst themselves (r^2>0.95). Sc-Ce (Fig. 8b) overlap with the field of both Group I and Group II cratonic eclogites, whereas Ce-Y variations overlap but extend to higher concentrations (Fig. 8d). The craton margin eclogites are more similar to Group I cratonic eclogites in terms of Ni versus Ce variation (Fig. 8a). As shown in Fig. 8c, a number of samples show distinct positive Eu anomalies (Eu/Eu*=1.5-2.0) and a couple show negative Eu anomalies (Eu/Eu*=0.67-0.8). Most samples with positive Eu anomalies also show

positive Sr anomalies (Sr/Sr* up to 9; where Sr* equals the interpolated value between Ce and Nd on a primitive mantle normalised diagram).

In terms of their trace element abundances, the garnet pyroxenite bulk rock compositions plot largely within the fields defined by the eclogites in Fig. 8, with the exception of Ni in garnet clinopyroxenite JJG2275 from Markt and Hf in garnet websterite 20043 from Jachtfontein, which are displaced to higher values. The garnet pyroxenites also do not show any significant Eu anomaly (Eu/Eu*=1.04±0.1).

The absence of reliable bulk rock data for Nb, Ta, Zr and Hf (all underestimated due to the contribution from rutile not being quantified), coupled with the likely low temperature mobility of at least Rb, and possibly Ba, makes depiction of primitive mantle normalised variations of limited value and provides little further information over the rare earth elements. Nevertheless, primitive mantle normalised variations in the eclogites and garnet pyroxenites are shown in Electronic Appendix 6 for interest. Although Zr and Hf concentrations are slightly underestimated, most samples show a modest negative Zr-Hf anomaly (greater than that likely due to rutile contribution based on published Zr and Hf analyses of rutile in eclogites (e.g. Aulbach *et al.*, 2011)) and two samples (20263 and 20293) from Jachtfontein show strong positive Zr-Hf anomalies. The garnet pyroxenites show similar primitive mantle normalised patterns to the eclogites, although garnet websterites 20770 and 20063 from Jachtfontein are distinct in being more depleted in trace elements, with mantle normalised abundances <1x primitive mantle values.

Chondrite normalised bulk-rock rare earth element abundances in the eclogite samples show generally systematic variations, and four distinct types of REE patterns can be recognised (Fig. 9). Type 1 have flat HREE patterns (7-20 x chondrite) and relative depletion in the LREE (La_n=2.6-6.7). These patterns are not unlike typical mid-ocean ridge basalt compositions. Type 2 patterns have been divided into two varieties both of which are convex-up. In Type 2a the maximum inflection point is at Sm, whereas for Type 2b it is at Nd. The LREEs in both show a positive slope (La_n=1.5-8, Sm_n=6-40 in Type 2a and in Type 2b La_n=2.8-25, Nd_n=20-76) and the HREE are depleted with a strong negative slope (Eu_n=7-43; Yb_n=2-11 in Type 2a and Sm_n=16-60; Yb_n=3.7-9 in Type 2b). Type 3 REE patterns are strongly depleted in both LREE (La_n=0.4-1.8) and HREE (Yb_n=2.4-4) with Eu showing highest normalised concentration (Eu_n=11-26); all Type 3 samples have positive Eu anomalies (Eu/Eu*=1.6-1.8). Type 4 REE patterns are particularly

unusual in having flat to concave-up LREEs, flat to convex-up and uniformly depleted HREEs, and positive Eu anomalies (Eu/Eu*=1.5-1.9).

GEOTHERMOBAROMETERY

There are relatively few mineral thermobarometers applicable to the mineralogically restricted assemblages characteristic of mantle-derived eclogites, and Fe-Mg exchange between clinopyroxene and garnet is most commonly used as a geothermometer. The formulation by Ellis and Green (1979) – referred to hereafter as EG79 and the formulation by Krogh (1988) (K88) have generally been the preferred choice for geothermometers applied to eclogites (e.g. Appleyard *et al.*, 2007, Jacob, 2004, Viljoen *et al.*, 2005), although more recent formulations such as those proposed by Krogh Ravna (2000) (KV00) and Nakamura (2009) (N09) have been argued by those authors to provide more reliable temperature estimates. In this study we have applied the EG79, K88, KR00 and N09 formulations to estimate temperature of equilibration of the eclogites, garnet clinopyroxenites and garnet websterites. In the eclogites, EG79 and K88 yielded temperatures that fall within 25^{o}C of each other and are strongly correlated (r^2=0.91), and thus for comparison purposes we report only EG79, KR00 and N09 in Table 6. The sensitivity of these Fe-Mg exchange geothermometers to Fe^{3+} content of the coexisting garnet and clinopyroxene is well known (e.g. Proyer *et al.*, 2004), but given the errors associated with estimating Fe^{3+} using stoichiometry, particularly in clinopyroxene, total iron as Fe^{2+} has been used in this study. In addition, application of these geothermometers requires an assumption of pressure, and thus depth of origin: temperatures have been calculated for assumed pressures of 3.0 GPa and 1.5 GPa, although for reasons discussed below the 1.5 GPa temperatures are believed to be more appropriate.

The calculated EG79 temperatures (at 1.5 GPa) for the eclogite samples range from 815 ^{o}C to 1000^{o}C (average=900±50^{o}C), whereas the Krogh Ravna (2000) temperatures are lower by some 100^{o}C (683-906 ^{o}C: average=790±60 ^{o}C). The N09 temperatures fall at intermediate values (747-988^{o}C: average=841±68^{o}C). At 3.0 GPa the EG79 temperatures range from 863 to 1051^{o}C (average=948±54 ^{o}C), and KR00 range from 771 to 1013^{o}C (average=886^{o}C, some 60 degrees cooler). Temperatures determined using N09 show a slightly wider range (812-1066 ^{o}C) but on average (910±73 ^{o}C) fall within error of EG79 temperatures. At 1.5 GPa the calculated EG79 temperatures for the garnet pyroxenite samples range from 686^{o}C to 835 ^{o}C (average=758±49 ^{o}C), whereas the Krogh Ravna (2000) temperatures are lower by some 100^{o}C (533-753 ^{o}C: average=640±73 ^{o}C). There is no statistically meaningful difference in calculated temperature

between the garnet clinopyroxenites and garnet websterites (Table 6). The N09 temperatures fall at intermediate values (583-829 ^{o}C: average=695±78 ^{o}C). At 3.0 GPa (Table 6) the EG79 temperatures range from 728 to 886 ^{o}C (average=804±52 ^{o}C), and KR00 range from 613 to 854 ^{o}C (average=730 ^{o}C; some 70 ^{o}C cooler). Temperatures determined using N09 show a slightly wider range (638-902 ^{o}C) but on average (758±83 ^{o}C) fall within the range of EG79 temperatures. Calculated temperatures of the garnet pyroxenites at 1.5 GPa are lower than for the eclogites by some 150 ^{o}C on average.

The pressure of last equilibration (and thus depth of origin) is not easy to determine on eclogites xenoliths due to their restricted mineralogy. In Fig. 10 the calculated temperatures (assuming 3.0 GPa pressure) are projected onto the Pollack and Chapman (1977) 40 mW.m^{-2} geotherm, that also corresponds to that obtained from peridotite xenoliths from kimberlite intrusions from the same craton margin (le Roex & Class, 2016). This approach places the eclogites squarely within the mantle at 100-130 km depth. In contrast, in his study of the eclogites and garnet granulites from this region, Robey (1981) argued on the basis of P-T pseudosections that the eclogites derived from pressures of 1.5-2.0 GPa, with the garnet granulites at the lower end of this range. Such pressures are more consistent with derivation from the lower crust.

Despite their restricted mineralogy, there have been some attempts at developing a geobarometer for mantle eclogite assemblages (Beyer *et al.*, 2015, Krogh Ravna & Terry, 2004, Sun & Liang, 2015). The craton margin eclogites from this study do not have suitable coexisting phases to apply the Krogh Ravna and Terry (2004) geobarometer, which requires phengite and quartz in addition to kyanite, garnet and clinopyroxene. The Beyer *et al.* (2015) geobarometer yields a very wide pressure range (0.5 to 4.0 GPa with a median of ~2.5 GPa), with the low end extending below the garnet stability field. At the calculated temperatures, a median pressure of 2.5 GPa would imply a shallow mantle origin and an ambient geotherm of some 50 mWm^{-2}. This is significantly higher than that determined from peridotite xenoliths from the same region (40 mW.m^{-2}; le Roex and Class, 2016), and would imply an unlikely mantle P-T disequilibrium scenario. Moreover, the same Beyer et al. (2015) geobarometer gives an identical pressure range and median (~2.5 GPa) for the on-craton eclogites from Roberts Victor, Kaalvallei and Lace (using published and unpublished data). Published, and generally accepted, pressures for these on-craton localities are in the range of 5 to 8 GPa (e.g. Aulbach & Viljoen, 2015, Viljoen *et al.*, 2005). The Beyer *et al.* (2015) geobarometer thus does not appear to provide useful information on depth of origin for these craton margin samples.

The recent geothermobarometer formulation by Sun and Liang (2015), which recognises that the partitioning of the REE between garnet and clinopyroxene is temperature and pressure dependant under equilibrium conditions, allows some insight into the possible depth of origin of these eclogites. The REE geobarometer requires equilibrium partitioning between garnet and clinopyroxene, and this condition appears to be met in most samples (Electronic Appendix 7 and 8). Cryptic metasomatism in particular can affect the light rare earth elements and lead to apparent disequilibrium conditions (e.g. le Roex & Class, 2016). Using the spreadsheet provided by Sun and Liang (2015) to calculate pressures for these craton margin eclogites met with mixed success, largely due to presence of non-equilibrium partitioning in roughly half the samples. Whereas the spreadsheet calculations are dependent on equilibrium being obtained between clinopyroxene and garnet in terms of their REE distributions it allows for deletion of individual rare earth elements where this condition appears not to have been met [i.e. where individual elements plot off the linear regression line in a plot of (lnD_i–Ai) vs. B_i – see definitions in Sun and Liang (2015)]. Although this decreases the associated error, it can significantly change the determined pressure and introduces a level of subjectivity to the calculated pressures. That said, and recognising this limitation, where garnet and clinopyroxene appear to be in equilibrium (generally none, but no more than three individual REE excluded from the correlation) calculated pressures (Table 6) range from 0.7 GPa to 2.6 GPa (average 1.7±0.4 GPa). The average of the calculated errors on each determination is 0.4 GPa. The equivalent pressure range for the garnet clinopyroxenites is 1.4±0.6 GPa, whereas that for the four garnet websterites is 1.4±0.5 GPa.

The garnet websterites have orthopyroxene present in addition to clinopyroxene and garnet and thus the more well established geobarometer of Taylor (1998) can be applied to these few samples. Calculated pressures using Taylor (1998) range from 1.4 to 2.6 GPa (average 1.8±0.5 GPa); a range that is, with the exception of sample 20043, in good agreement with that determined using the Sun and Liang (2015) REE geobarometer for the same samples (Table 6).

By comparison, using the same REE partitioning approach, pressures calculated for on-craton Group I Roberts Victor, Jagersfontein and Jwaneng eclogites (unpublished data) and off-craton peridotites from the same craton margin region (le Roex & Class, 2016) are systematically higher, with the majority in the range 3.0-4.0 GPa, but extending to ~7.0 GPa . The systematically higher calculated pressures for the on-craton eclogites using the Sun and Liang (2015) geobarometer is

taken to imply that the lower 1-2 GPa pressures (and thus depths of origin) of the craton margin eclogites are possibly a reasonable indication of depth of last equilibration.

Adopting a pseudosection approach using Thermocalc (Powell *et al.*, 1998), and using calculated bulk rock compositions, modal mineralogy, mineral compositions and calculated temperatures of equilibration, results in similar pressures of equilibration to those obtained with the Sun and Liang (2015) REE geobarometer. For the calculated range of temperatures of equilibration (Table 6), the bimineralic eclogite assemblage stabilises at 1.3 to 1.6 GPa, the kyanite eclogite assemblages at 1.7 to 2.2 GPa, and the garnet pyroxenites at 0.9 to 1.0 GPa. This generally good agreement with the Sun and Liang (2015) REE pressures lends some credence to the latter.

DISCUSSION

Comparison to on-craton eclogite xenoliths

Petrographically, the craton margin eclogite xenoliths from this study are largely indistinguishable from mantle eclogites from locations on the Kaapvaal craton. Textures include both Group I and Group II varieties, a similar range in grain size, and the same suite of accessory minerals are present, primarily rutile and some kyanite, with very minor phlogopite or sanidine. Granoblastic textures dominate, and mineralogical banding is common. Straight grain boundaries and 120^{o} triple junctions attest to near equilibrium textures. Late stage amphibole and phlogopite frequently occur along fractures and grain boundaries. Mineral compositions overlap (Figs. 3 & 4), and the very low K_2O contents in clinopyroxene and Na_2O contents in garnet strongly indicate a Group II classification. The common decomposition of jadeite-rich clinopyroxene of cratonic kyanite eclogites to a fine-grained indeterminate mixture (e.g. Berg, 1968, Smyth, 1980) is, however, not observed in these craton margin kyanite eclogites. This may indicate derivation from lower pressures.

Reconstructed bulk rock major element compositions for the craton margin eclogite xenoliths are basaltic in nature and show closer affinity to Group I than to Group II on-craton eclogite xenoliths from southern Africa (Fig.7). When compared to the Rietfontein off-craton eclogites, these craton margin eclogites display clear differences in composition, with the bimineralic eclogites from Rietfontein being more MgO-rich, and the kyanite eclogites having lower SiO_2 and FeO (at given MgO) but higher CaO and Al_2O_3 (Fig. 7). Although there is overlap, cratonic eclogites tend to have higher Ni concentrations (up to 520 ppm; Fig.8) than the craton margin eclogites (Ni<200 ppm; sample 02200 with 296 ppm excepted). Chondrite normalised REE patterns similarly

provide some clear differences. Eclogites from Roberts Victor, Kaalvallei and Lace (this study unpublished, Aulbach & Viljoen, 2015, Dludla *et al.*, 2006, Viljoen *et al.*, 2005) differ in their chondrite normalised HREE abundance patterns from the craton margin eclogites (bar those with Type 1 REE patterns) in having ubiquitous flat HREE patterns with associated slight depletion in LREE with or without Eu anomalies (La_n = 0.75-6; Yb_n = 3-20). The off-craton eclogites from Rietfontein have similar flat HREE patterns (Appleyard *et al.*, 2007). Whereas the Type 1 REE patterns from these craton margin eclogites are similar to those from on-craton locations, the remaining Types 2 to 4 differ in having HREE patterns with characteristic negative slopes (i.e. relative depletion towards Yb), and moderately to heavily depleted LREEs (Fig. 9). Type 4 REE patterns are particularly unusual in having flat (but low) HREE abundances and concave-up LREE patterns (Fig. 9).

Perhaps the most significant difference, at least relative to Kaalvallei and Orapa on-craton Group I eclogites, is found in the Sr-Nd isotope compositions. On a plot of $^{143}Nd/^{144}Nd$ versus $^{87}Sr/^{86}Sr$, clinopyroxenes from the craton margin eclogites and garnet pyroxenites, with two exceptions (42123 and 42143), plot well below the 'mantle array' (Fig. 6a). Although Sr and Nd were only measured in clinopyroxene, the bulk rock Sr isotope ratios will not differ significantly given the negligible Rb and Sr in garnet, and despite the high Sm/Nd ratio of garnet Nd isotope ratios will not differ by more than ~1 in the fourth decimal place for the samples in question (assuming initial equilibrium between clinopyroxene and garnet) given the very low absolute concentrations of Nd in the analysed garnets. The bulk rock $^{143}Nd/^{144}Nd_i$ and $^{87}Sr/^{86}Sr_i$ ratios will thus similarly plot below the mantle array. The two Roodekraal xenoliths that plot close to the mantle array within the 'depleted quadrant' also plot very close to the field of off-craton Group I kimberlites, indicating that their clinopyroxene isotope compositions may have been compromised by the host kimberlite. As might be expected of mantle eclogites with purported oceanic basalt protoliths, clinopyroxenes from the Kaalvallei and Orapa Group I eclogites reported on by Viljoen *et al.* (2005), Viljoen *et al.* (1996) plot within the mantle array.

Nature and origin of protoliths

Eclogite xenoliths hosted in kimberlites are usually attributed to one of two origins. The first, linked to so-called Group I eclogites, is via prograde metamorphism of recycled (Archean) oceanic crust, with or without melt loss associated with subduction (e.g. Aulbach & Jacob, 2015, Aulbach *et al.*, 2017, Aulbach & Viljoen, 2015, Barth *et al.*, 2001, Barth *et al.*, 2002, Jacob *et al.*, 1994, Jacob, 2004, Jacob *et al.*, 2005, Shirey *et al.*, 2001, Snyder *et al.*, 1997, Viljoen *et al.*, 2005,

Viljoen *et al.*, 1996). The second, linked to so-called Group II eclogites, is *in situ* formation in the lithospheric mantle via crystallization of a primary mantle melt at high pressure (e.g. Viljoen *et al.*, 2005). In short, Group I eclogites are oceanic crustal rocks (basalt or gabbro; possibly mixed with sediment) that have experienced deep (ancient) recycling and high-grade metamorphism to eclogite facies prior to attachment to the continental lithospheric mantle. Less frequently it has been argued that eclogite xenolith suites have formed via reaction of a tonalitic/carbonatitic melt with mantle peridotite above a subduction zone (Barth *et al.*, 2002, Snyder *et al.*, 1997, Taylor & Neal, 1989, Taylor *et al.*, 2003, Viljoen *et al.*, 1996), or that they represent residues of tonalite melt extraction from Archean continental mafic crust, with subsequent foundering of the lower crust into the underlying lithospheric mantle (e.g. Koidu, West Africa; Barth *et al.*, 2001, Rollinson, 1997).

There are several lines of evidence that point to the likelihood that the protoliths to these craton margin eclogites and garnet pyroxenites were neither once mid-ocean ridge basalt that has passed through a subduction zone before being incorporated into the overlying lithospheric mantle, nor the product of crystallisation of high pressure mafic melts at mantle depth. The recalculated bulk rock eclogite compositions are mafic, but poor in SiO_2 compared to present day (and presumably Archean) mid-ocean ridge basalts. However, the low silica could reflect removal of a melt phase during subduction (e.g. Snyder *et al.*, 1997, Taylor *et al.*, 2003) or during prograde metamorphism in the crust (e.g. Rollinson, 1997) so is not diagnostic (some 10% removal of a felsic melt with 70% SiO_2 would lower the SiO_2 from ~50 wt.% to 47 wt.%). Many of the eclogites show positive Eu anomalies (Eu/Eu*=1.5-1.9), and some show negative Eu anomalies (Eu/Eu* down to 0.67), indicating that plagioclase enrichment, or fractionation, played a role in their early history; i.e. their magmatic protoliths were once at crustal levels. From a petrological perspective, sample 20720 from Jachtfontein is a composite sample showing part garnet granulite and part eclogite, with a clear contact between the two different lithologies (Fig. 2b). The eclogite component is compositionally no different from the other eclogite samples analysed and this sample at least appears to be unquestionably from the lower continental crust.

Reconstituted chondrite normalised bulk rock REE abundances in the eclogites and garnet pyroxenites include patterns similar to typical basalt (mid-ocean ridge or continental; Type 1, Fig. 11a), patterns that are unusual in having sinusoidal shapes (Type 2a; Fig. 11, Type 2b; Fig. 11b,), patterns with negatively sloped HREE coupled with positively sloped LREE (Type 3; Fig. 11c), or have flat but strongly depleted HREE and concave-up LREE (Type 4; Fig. 11d). Eclogite xenolith

suites that have been argued to have recycled mafic oceanic crust as a protolith (e.g. cratonic eclogites) tend to have flat HREE and slightly depleted LREE patterns (e.g. Appleyard *et al.*, 2007, Dludla *et al.*, 2006, Viljoen *et al.*, 2005) consistent with REE patterns shown by mid-ocean ridge basalts. Importantly, they retain the REE pattern of their original igneous protolith despite the impact of subduction zone processes en route to being incorporated into the lithospheric mantle. Amongst the four types of REE patterns identified (Fig. 11), only Type 1 patterns mimic those found in basaltic magmas (Fig. 11a) and are similar to typical geochemically depleted mafic magmas (basalt or gabbro) with flat HREE (~10 x chondrite) and flat to depleted LREE at around 5-10 x chondrite. In contrast, Type 2, 3 and 4 REE patterns are not reflective of reasonably undisturbed mantle derived mafic magmas and must have experienced a more complex petrogenetic history. In this regard, it is noteworthy that three of the four types of REE patterns (Types 1, 2 and 4 in Fig. 11) can be found amongst the associated garnet granulite xenoliths, and the absence of Type 3 might be nothing more than a sampling problem given the relatively few garnet granulites available for comparison. The strong likelihood is that the direct protoliths of these craton margin eclogites and garnet pyroxenites were thus lower crustal mafic garnet granulites which underwent high-grade metamorphism to eclogite facies, retaining the REE pattern of their garnet granulite protolith.

The bulk rock REE compositions were based on the observed modal mineralogy of the eclogites, garnet pyroxenites and garnet granulites. One might argue that the unusual Type 2, 3 and 4 REE patterns are reflective of a missing component, and it is true that addition of zircon (strongly HREE enriched) plus apatite (strongly LREE enriched) has the ability to flatten out the REE patterns to resemble something more akin to the REE pattern of a mafic magma. However, there is no evidence of zircon in any of the samples (despite searching with mapping software on the electron microprobe) and apatite has been found in only three samples – two of which have Type 2b REE patterns and one Type 1. There is thus little basis to attribute the unusual patterns to absence of zircon and apatite in the bulk rock calculations.

Sr-Nd isotope compositions provide further evidence for protoliths that are distinct from recycled ancient oceanic crust in that they plot below the mantle array and notably within the field of Namaqua-Natal Belt lower crust (Fig. 6a). In contrast, cratonic (Group I) eclogites plot within or close to the mantle Sr-Nd array (Fig. 6a) and appear thus to have retained the broad Sr-Nd systematics of their protolith during the oceanic crust recycling process. In terms of Sr-Pb isotope variations, these craton margin samples similarly plot within the field for Namaqua-Natal Belt

lower crust, although the garnet pyroxenites plot in the area of overlap with MORB (Fig. 6b). The overlap in oxygen isotope ratios between the eclogite/garnet pyroxenite xenoliths and the garnet granulites xenoliths analysed in this study is consistent with this interpretation (Fig. 6c).

Finally, although the data are scattered, the low (1.0-2.0 GPa) calculated pressures of last equilibration using the Sun and Liang (2015) REE geobarometer point to a lower crustal origin rather than mantle origin for these xenoliths. Depending on whether one uses the EG79 or KR00 calculated temperatures, the P-T trajectory of these eclogites corresponds to a geothermal gradient of between 70 and 80 $mW.m^{-2}$ (Fig. 10) considerably higher than that obtained for the underlying mantle of ~40 $mW.m^{-2}$ (le Roex & Class, 2016), but broadly consistent with, although slightly higher than, the measured present-day average heat flow of 61 ± 11 $mW.m^{-2}$ of the Namaqua-Natal Belt (Jones, 1987). The garnet pyroxenites show a slightly lower temperature range at equivalent pressure relative to the eclogites and plot closer to the 60-70 $mW.m^{-2}$ geothermal gradient, depending on which geothermometer one uses, but still significantly higher than the underlying mantle geotherm. Taken together with the geochemical evidence, these craton margin eclogites and garnet pyroxenites are unlikely to represent recycled oceanic crust incorporated into the continental lithospheric mantle, and their protoliths are more likely to have been mafic lower crustal rocks from the underlying Namaqua-Natal Belt.

The original tectonic setting into which the precursor igneous rocks to these eclogites and garnet pyroxenites was emplaced is difficult to discern with confidence. Comparison of bulk compositions to typical within-plate and plate margin magma compositions is unproductive given the extremely large number of analyses now available through database such as GeoRoc and PetDB. This plethora of data leads to very large scattered fields for the different rock types that overlap significantly and are thus not objectively discriminatory. In the absence of reliable information on key elements such as Nb, Ti, Ta (all hosted by the heterogeneously distributed accessory phase rutile), which facilitate distinguishing between within-plate and destructive margin settings, application of discrimination diagrams using these elements is not possible. In terms of major elements the bulk rock compositions define an iron-enrichment trend on an AFM diagram, suggesting possible allegiance to a constructive or within plate setting.

Whether these eclogites date back to the lower crust that existed prior to collision of the Namaqua-Natal Belt with the Kaapvaal craton at ~1.1 Ga, or whether they developed as a result of the collision and associated crustal thickening is not known. There is some evidence for the former in

that Schmitz and Bowring (2000) have shown that zircon from a single Lovedale eclogite (not analysed in this study) gives a ~2.6 Ga peak metamorphic age. Alternatively, if related to ultra-metamorphism during the Namaqua-Natal orogeny, then a number of studies (e.g. Cornell *et al.*, 2006 and references therein) have argued that prior to collision with the Kaapvaal craton the Namaqua-Natal Belt comprised a series of stacked arc terranes which would suggest mafic calc-alkaline precursors.

Namaqua-Natal Belt lower crust

The exact boundary between the Kaapvaal craton and the Proterozoic Namaqua-Natal Belt to the south is poorly constrained. In the southwest, it is taken as the Brakbos Fault (e.g. Schmitz & Bowring, 2004) which can be mapped to about 30º south, close to the Markt kimberlite sample locality which lies to the west. Markt is thus clearly off-craton. The fault is not exposed further to the southeast and its location has been inferred from aeromagnetic lineaments extending in an east-southeastly direction. Pearson *et al.* (1995) and Schmitz and Bowring (2004) place Lovedale slightly on-craton, and Pearson *et al.* (1995) place Jachtfontein off-craton. Given the relative positions, Roodekraal would then be slightly on-craton. However, the inferred craton boundary effectively runs parallel to the trend of these three kimberlites in an east-southeasterly direction, and the N-S displacement of the kimberlites is only some 35 km; less than the uncertainty of the exact location of the craton margin. In this regard, all three localities could equally be on- or off-craton. Given the abundance of garnet granulites at all three locations, and the purported scarcity of such lithologies as xenoliths found in kimberlites on the Kaapvaal craton (e.g. Griffin *et al.*, 1979), coupled with the seismic evidence from Nguuri *et al.* (2001) which shows that the craton has uniformly thinner crust (35-40 km) than the adjacent Namaqua-Natal Belt (40-45 km), it is proposed that all three localities are in fact marginally off-craton. The recovered xenoliths are thus interpreted to be samples of the lowermost regions of the underlying Namaqua-Natal Belt lower crust, as illustrated schematically in Fig. 12.

The inferred geotherm determined from the eclogite samples extends the off-craton paleo-geotherm for the Namaqua-Natal Belt of Pearson *et al.* (1995) based on granulite P-T equilibration (also using EG79) to higher pressures (Fig. 10). The calculated geotherm is clearly much higher than the steady state conductive geotherm of ~40 $mW.m^{-2}$ constructed for the underlying mantle (le Roex & Class, 2016). It is thus not interpreted as a paleo-geotherm at the time of kimberlite emplacement, but rather reflects higher P-T crustal conditions that were "frozen-in" soon after the prograde metamorphism and crustal thickening in the region at the time of collision of the

Namaqua-Natal Belt with the Kaapvaal craton. The marginally lower P-T conditions shown by the garnet pyroxenites suggest that these slightly more magnesian compositions continued to re-equilibrate to lower temperatures, before also being frozen in.

Pressures of equilibration of these craton margin eclogites are not well constrained, but as discussed above best estimates suggest that they originate from 45-55 km depth (depending on the assumed crustal density). This contrasts somewhat with the inferred crustal thickness beneath the region of sampling, based on seismic evidence, which suggests a slightly thinner crust of 40-45 km thickness (Nguuri *et al.*, 2001) thickening southward. However, it is well known that the petrological crust-mantle boundary can be significantly deeper than the seismic Moho when substantial crustal eclogite is present, due to eclogite having similar Vp (~7.8 km/s) to mantle peridotite (e.g. Griffin & O'Reilly, 1986, Mengel & Kern, 1992). It is therefore suggested that the petrological crust-mantle boundary in the region is deeper by some 5-8 km than the seismic Moho.

From their study on zircons from garnet granulites from the same region, Schmitz and Bowring (2000, 2004) argued that granulitization of the lower Namaqua-Natal crust occurred at ~1.1 Ga, affecting pre-existing Archean and Mesoproterozoic crust. These authors argue further that the nature of granulite metamorphism was more consistent with crustal thickening relating to collisional orogenesis than with underplating by mafic magmas. Whether the eclogites formed during the same process or whether they reflect ancient remnants in the otherwise Early Proterozoic plate prior to collision with the Kaapvaal craton at 1.1 Ga remains unclear. At least some pre-existed the Namaqua-Natal orogeny in that zircon from a single eclogite from Lovedale gave a late Archean age (~2.6 Ga; Schmitz & Bowring, 2000). The eclogites analysed in this study define a Sm-Nd "errorchron" ($r^2 = 0.96$) with an age of ~900 Ma that is close to the ~1.0 Ga age determined for Namaqua-Natal Belt granulites by Schmitz and Bowring (2004) consistent with eclogite formation relating to the same orogenic event. However, this ~1 Ga age could reflect resetting during the high-grade metamorphism of the Namaqua-Natal orogeny.

SUMMARY

Thirty-three eclogite and ten garnet pyroxenite xenoliths hosted in five kimberlites (Goedehoop, Jachtfontein, Lovedale, Markt and Roodekraal) emplaced along the southern margin of the Kaapvaal craton have been studied to determine the nature of their protoliths and their petrogenetic history.

1. The eclogite and garnet pyroxenite xenoliths are primarily bimineralic with accessory rutile, but kyanite eclogites are present at the Lovedale and Roodekraal localities. Based on K_2O in clinopyroxene and Na_2O in garnet the eclogites are best classified as Group II.
2. Textures are largely granoblastic and mineralogical banding is common. Calculated temperatures and pressures of equilibration of the eclogites (700-1000 °C; 1.5±0.5 GPa) suggest that they were sampled by the host kimberlite from depths of 50-55 km. Garnet pyroxenites give slightly lower temperatures (686-835 ^{o}C) at similar pressures.
3. Reconstituted bulk rock compositions of the eclogites, assuming clinopyroxene and garnet in equal proportions, indicate the precursor rocks were mafic in composition, and chondrite normalised REE patterns show that some have significant positive Eu anomalies, indicating a mafic protolith relatively enriched in plagioclase. Four distinct groups of chondrite normalised REE patterns can be recognised amongst the xenolith suite. Type 1 is consistent with derivation from a normal slightly LREE depleted basaltic precursor, with flat HREE patterns. The remainder have more complex chondrite normalised REE patterns including sinusoidal patterns, concave-up LREE, and positive sloped LREE coupled with negative sloped HREE, collectively unlike typical igneous rocks or Group I eclogites from the Kaapvaal craton.
4. A genetic link between the eclogite/pyroxenite xenoliths and the associated garnet granulite xenoliths is suggested by the similar chondrite normalised REE patterns found in both groups of rocks, and in one sample (20720) with shared lithological contact. $^{143}Nd/^{144}Nd$ and $^{87}Sr/^{86}Sr$ isotope ratios of the eclogites and garnet clinopyroxenites fall well below the mantle array and overlap the field for lower crustal samples from the Namaqua-Natal Belt.
5. Prograde metamorphism of the mafic garnet granulite protoliths to these eclogites and garnet pyroxenites is inferred to have occurred during crustal shortening and thickening associated with the collision of the Namaqua-Natal Belt with the Kaapvaal craton at 1-1.2 Ga, although some could be remnants existing in the Early Proterozoic lower crust prior to collision with the Kaapvaal craton.

FUNDING

This work was funded by the National Research Foundation of South Africa (grant 68919 to AlR) and from the Centre National de la Recherche Scientifique (INSU grant to MG).

ACKNOWLEDGEMENTS

For the stable oxygen isotope analyses undertaken in the isotope laboratory of the University of Lausanne, the assistance of Torsten Vennemann is much appreciated. The hospitality of the owners of Lovedale, Jachtfontein, Markt and Roodekraal farms made sampling possible and is gratefully acknowledged. Jock Robey is thanked for his invaluable assistance in the field. We thank Sonia Aulbach, Fanus Viljoen and the editor, Jörg Hermann, for their critical comments which improved the final version of this manuscript. Johann Diener is thanked for determining pseudo-sections using Thermo-Calc.

FIGURE CAPTIONS

Figure 1: Map showing the location of Jachtfontein (J), Lovedale (L), Markt, Roodekraal (R) and Goedehoop (G) kimberlites relative to the Kaapvaal craton and Namaqua-Natal Belt. The on-craton eclogite locality of Roberts Victor and the off-craton Rietfontein locality are also shown.

Figure 2: Selected photomicrographs showing salient features of selected eclogite xenoliths. (a) Eclogite 026203L from Lovedale, (b) Eclogite 20720 from Jachtfontein showing contact between eclogite (20720e) on the right and garnet granulite (20720g) on the left, (c) Eclogite 10063 from Markt, (d) Kyanite eclogite 42123 from Roodekraal.

Figure 3: (a) Ca# (atomic Ca/Ca+Fe+Mn+Mg) versus Mg# (atomic Mg/Mg+Fe) in garnets from craton margin eclogites. Classification boundaries from Aulbach *et al.* (2017). Field for on-craton eclogites includes data from Roberts Victor (Hatton, 1978), Jagersfontein and Jwaneng (this study), Lace (Aulbach & Viljoen, 2015), Orapa (Shee, 1978), Kaalvallei (Viljoen *et al.*, 2005). (b) K_2O (wt.%) in clinopyroxene versus Na_2O (wt.%) in garnet for craton margin eclogites showing Group I and Group II boundaries from McCandless and Gurney (1989). Field for on-craton eclogites as for (a).

Figure 4: (a) Ca-Mg-Fe compositional variation of clinopyroxene and garnet in craton margin eclogites, garnet clinopyroxenites and garnet websterites. (b) Na_2O–MgO (wt.%) variation in clinopyroxene from craton margin eclogites. Group A, B and C subdivisions from (Taylor & Neal, 1989). (c) Compositional variation of craton margin eclogites with respect to Diopside-Jadeite-Aegirine. Ferric iron calculated following Droop (1987). Field for on-craton eclogites as for Fig. 3. Symbols for eclogites in all three panels as for Fig. 3; garnet clinopyroxenites: red open squares; garnet websterites: red open squares with solid centre.

Figure 5: Chondrite normalised REE diagrams for clinopyroxene (solid circles) and garnet (open circles) in representative craton margin eclogites from Lovedale (a), Markt (b), Jachtfontein (c) and Roodekraal (d). Chondrite normalising values from (Sun & McDonough, 1989).

Figure 6: (a) Initial $^{143}Nd/^{144}Nd$ versus $^{87}Sr/^{86}Sr$ isotope ratios measured in clinopyroxene from craton margin eclogites and garnet pyroxenites. Symbols as in Figure 4. Where Nd isotope data are not available (for laser ablation determined $^{87}Sr/^{86}Sr$) data have been plotted on the x-axis at $^{143}Nd/^{144}Nd = 0.5112$ to show range in $^{87}Sr/^{86}Sr$. Initial ratios calculated for age of kimberlite pipe. Two sigma error bars are shown or are less than symbol size. Field for off-craton Group I kimberlites from Becker and le Roex (2006). Field for Namaqua-Natal Belt (NNB) lower crust from Class and le Roex (2011), Huang *et al.* (1995) and this study. Field for clinopyroxenes from Kaalvallei eclogites from Viljoen *et al.* (2005). (b) Initial $^{87}Sr/^{86}Sr$ versus $^{206}Pb/^{204}Pb$ measured in clinopyroxene from craton margin eclogites and garnet pyroxenites. Two sigma error bars are shown, or are less than symbol size. MORB field shown schematically. Field for Namaqua-Natal Belt (NNB) lower crust from Class and le Roex (2011), Huang *et al.* (1995) and this study. (c) Oxygen isotope ratios (in ‰) in craton margin eclogites, garnet pyroxenites and garnet granulites. $\delta^{18}O$ data for other eclogite localities from Jacob (2004 and references therein).

Figure 7: Variations in selected major elements from reconstructed bulk rock compositions for craton margin eclogites and garnet pyroxenites. Symbols as in Figure 4. The few kyanite eclogites are shown with half-filled circles. Field for off-craton Rietfontein eclogites (Rftn) and Rietfontein kyanite eclogites (Rftn KE) from Appleyard *et al.* (2007). Fields for Group I and Group II on-craton eclogites in grey from Viljoen *et al.,* (2005), Aulbach and Viljoen (2015), Hatton (1978), Shee (1978), this study.

Figure 8: Variation in selected trace elements from reconstructed bulk rock compositions for craton margin eclogites and garnet pyroxenites. Symbols as in Figure 4. Eu*= chondrite normalised $Eu/(Sm^{1/2}*Gd^{1/2})$. Field for off-craton Rietfontein eclogites from Appleyard *et al*. (2007). Fields for Group I and Group II on-craton eclogites from Viljoen *et al.* (2005), Aulbach and Viljoen (2015), Hatton (1978), Shee (1978) and this study.

Figure 9: Chondrite normalised REE patterns in reconstructed bulk rock compositions of eclogites and some garnet pyroxenites. Samples have been subdivided into four types with distinctive patterns. See text for further discussion. Chondrite normalising values from Sun and McDonough (1989). Solid symbols: eclogites; open symbols: garnet pyroxenites.

Figure 10: P-T diagram showing calculated equilibrium temperatures for the craton margin eclogites plotted against the 40 $mW.m^{-2}$ geotherm (Pollack & Chapman, 1977) – dashed black line, and parallel to the geotherm slope using an average of 1.5 GPa pressure – solid black line, using Ellis and Green (1979). Calculated equilibrium temperatures for garnet pyroxenites (assuming 1.5 GPa pressure) lie along the 70 $mW.m^{-2}$ geotherm (short and long dashes). Also shown is the field of calculated equilibrium pressures and temperatures for peridotite xenoliths from craton margin kimberlites (le Roex & Class, 2016) and the P-T field for garnet granulites from the Namaqua-Natal Belt (Pearson *et al.*, 1995). Graphite-diamond boundary from (Kennedy & Kennedy, 1976).

Figure 11: Fields highlighting the four different chondrite normalised REE patterns recognised amongst reconstructed bulk rock compositions of craton margin eclogites and garnet pyroxenites with superimposed REE patterns from selected garnet granulite xenoliths from this study. Reconstructed bulk rock compositions of the garnet granulite xenoliths calculated using modal abundances in analysed samples. (a) Type 1 REE patterns with superimposed pattern of garnet granulite GHP03 and an example of a continental gabbro without Eu anomaly. (b) Type 2b REE pattern with superimposed REE patterns of garnet granulites HGX07 and GHP01. (c) Field of Type 3 REE patterns. (d) Type 4 REE pattern with superimposed REE pattern of garnet granulite 02GG15. Chondrite normalising values from Sun and McDonough (1989).

Figure 12: Schematic cross-section of the Namaqua-Natal Belt crust beneath the region of study, showing eclogite and garnet pyroxenite lithologies extending below the seismic Moho. Modified from Hawkesworth and Kemp (2006).

Electronic Appendix 1: Plot of $^{87}Sr/^{86}Sr$ determined in clinopyroxenes by laser ablation MC-ICP-MS versus $^{87}Sr/^{86}Sr$ determined on solutions from dissolution of a mineral separate from the same sample by MC-ICP-MS. Analytical conditions as described in the text. Error bars reflect two sigma errors. Errors are less than symbol size for solution analysis.

Electronic Appendix 2: Summary table of garnet granulite petrography

Electronic Appendix 3: Clinopyroxene and garnet analyses from garnet granulites

Electronic Appendix 4: Chondrite normalised REE patterns in clinopyroxene (solid circles) and garnet (open circles) in garnet clinopyroxenite (a) and garnet websterite (b) xenoliths from craton margin localities. Chondrite normalising values from Sun and McDonough (1989).

Electronic Appendix 5: Recalculated bulk rock compositions of garnet pyroxenites. Compositions calculated using determined modal mineralogy and analysed mineral compositions.

Electronic Appendix 6: Primitive mantle normalised trace element variations in reconstructed bulk rock compositions of craton margin eclogites. Field for Lovedale eclogites is shown in grey for clarity. Bulk rock compositions have been calculated assuming equal garnet and clinopyroxene, modified by the calculated amount of rutile necessary to remove any evidence of a negative Ti anomaly. In the absence of Zr and Hf data for rutile, the values for these elements are slightly underestimated (although on the scale of the y-axis, unlikely to be visually significant). Primitive mantle normalising values from Sun and McDonough (1989).

Electronic Appendix 7: $D^{cpx/gt}$ versus rare earth element for craton margin eclogites showing equilibrium partitioning. Data for off-craton peridotites from le Roex and Class (2016).

Electronic Appendix 8: Calculated clinopyroxene-garnet partition coefficients for the rare earth elements La, Ce, Nd and Gd versus equilibrium temperature calculated using the geothermometer of Ellis and Green (1979) for samples showing equilibrium relations.

References

Appleyard, C. M., Bell, D. R. & le Roex, A. P. (2007). Petrology and geochemistry of eclogite xenoliths from the Rietfontein kimberlite, Northern Cape, South Africa. *Contributions to Mineralogy and Petrology* **154**, 309-333.
Aulbach, S., Gerdes, A. & Viljoen, K. S. (2016). Formation of diamondiferous kyanite–eclogite in a subduction me´lange. *Geochimica et Cosmochimica Acta* **179**, 156-176.
Aulbach, S. & Jacob, D. E. (2015). Major- and trace-elements in cratonic mantle eclogites and pyroxenites reveal heterogeneous sources and metamorphic processing of low-pressure protoliths. *Earth and Planetary Science Letters* **431**, 274-286.

Aulbach, S. & Jacob, D. E. (2016). Major- and trace-elements in cratonic mantle eclogites and pyroxenites reveal heterogeneous sources and metamorphic processing of low-pressure protoliths. *Lithos* **262**, 586-605.
Aulbach, S., Jacob, D. E., Cartigny, P., Stern, R. A., Simonetti, S. S., Worner, G. & Viljoen, K. S. (2017). Eclogite xenoliths from Orapa: Ocean crust recycling, mantle metasomatism and carbon cycling at the western Zimbabwe craton margin. *Geochimica et Cosmochimica Acta* **213**, 574-592.
Aulbach, S., O'Reilly, S. Y. & Pearson, N. J. (2011). Constraints from eclogite and MARID xenoliths on origins of mantle Zr/Hf–Nb/Ta variability

Contributions to Mineralogy and Petrology **162**, 1047-1062.
Aulbach, S. & Viljoen, K. S. (2015). Eclogite xenoliths from the Lace kimberlite, Kaapvaal craton: From convecting mantle source to palaeo-ocean floor and back. *Earth and Planetary Science Letters* **431**, 274-286.
Barth, M. G., Rudnick, R. L., Horn, I., McDonough, W. F., Spicuzza, M. J. & Valley, J. W. (2001). Geochemistry of xenolithic eclogites from West Africa; Part I, A link between low MgO eclogites and Archean crust formation. *Geochimica et Cosmochimica Acta* **65**, 1499-1527.
Barth, M. G., Rudnick, R. L., Horn, I., McDonough, W. F., Spicuzza, M. J., Valley, J. W. & Haggerty, S. E. (2002). Geochemistry of xenoliths from West Africa, part 2: Origins of the high MgO eclogites. *Geochimica et Cosmochimica Acta* **66**, 4325-4345.
Becker, M. & le Roex, A. P. (2006). Geochemistry of South African on- and off-craton, Group I and Group II kimberlites: petrogenesis and source region evolution. *Journal of Petrology* **47**, 673-703.
Berg, G. W. (1968). Secondary alteration in eclogites from kimberlite pipes. *American Mineralogist* **53**, 1336-1346.
Beyer, C., Frost, D. J. & Miyajima, N. (2015). Experimental calibration of a garnet-clinopyroxene gebarometer for mantle eclogites. *Contributions to Mineralogy and Petrology* **169**.
Class, C. & le Roex, A. P. (2011). South Atlantic DUPAL anomaly — Dynamic and compositional evidence against a recent shallow origin. *Earth and Planetary Science Letters* **305**, 92-102.
Copeland, S. R., Sponheimer, M., le Roux, P. J., Grimes, V., Lee-Thorp, J. A., de Ruiter, D. J. & Richards, M. P. (2008). Strontium isotope ratios (87Sr/86Sr) of tooth enamel: a comparison of solution and laser ablation multicollector inductively coupled plasma mass spectrometry methods. *Rapid Communications in Mass Spectrometry* **22**, 3187-3194.
Cornell, D. H., Thomas, R. J., Moen, H. F. G., Reid, D. L., Moore, J. M. & Gibson, R. L. (2006). The Namaqua-Natal Province. In: Johnson, M. R., Anhaeusser, C. R. & Thomas, R. J. (eds.) *The Geology of South Africa*: Geological Society of South Africa, 325-379.
Dludla, S., le Roex, A. P. & Gurney, J. J. (2006). Eclogite xenoliths from the Premier kimberlite, South Africa: geochemical evidence for a subduction origin. *South African Journal of Geology* **109**, 353-368.
Droop, G. T. R. (1987). A general equation for estimating Fe^{3+} concentrations in ferromagnesian silicates and oxides from microprobe analyses, using stoichiometric criteria. *Mineralogical Magazine* **51**, 431-435.
Ellis, D. J. & Green, D. H. (1979). An experimental study of the effect of Ca upon garnet-clinopyroxene Fe-Mg exchange equilibria. *Contributions to Mineralogy and Petrology* **71**, 13-22.
Galer, S. J. G. & Abouchami, W. (1998). Practical applictaion of lead triple spiking for correction of instrumental mass discrimination. *Mineralogical Magazine* **62A**, 492-492.
Griffin, W. L., Carswell, D. A. & Nixon, P. H. (1979). Lower crustal granulites from Lesotho, South Africa. In: Boyd, F. R. & Meyer, H. O. A. (eds.) *The Mantle Sample: Inclusions in Kimberlites and other Volcanics*. Washington, D.C.: American Geophysical Union, 59-86.

Griffin, W. L. & O'Reilly, S. Y. (1986). The lower crust in eastern Australia: xenolith evidence. *Geological Society Special Publication* **24**, 363-374.
Harris, C., le Roux, P., Cochrane, R., Martin, L., Duncan, A. R., Marsh, J. S., le Roex, A. P. & Class, C. (2015). The oxygen isotope composition of Karoo and Etendeka picrites: High δ18O mantle or crustal contamination? *Contributions to Mineralogy and Petrology* **170:8**.
Harris, C. & Vogeli, J. (2010). Oxygen isotope composition of garnet in the Peninsula granite, Cape granite suite, South Africa: Constraints on melting and emplacement mechanisms. *South African Journal of Geology* **113.4**, 401-412.
Harris, M., le Roex, A. & Class, C. (2004). Geochemistry of the Uintjiesberg kimberlite, South Africa: petrogenesis of an off-craton, group I, kimberlite. *Lithos* **74**, 149-165.
Hart, S. R. (1984). A large-scale isotope anomaly in the Southern Hemisphere mantle. *Nature* **309**, 753-757.
Hatton, C. (1978). The geochemistry and origin of eclogites from the Roberts Victor mine. Cape Town.
Hawkesworth, C. J. & Kemp, A. I. S. (2006). The differentiation and rates of generation of the continental crust. *Chemical Geology* **226**, 134-143.
Huang, Y.-M., van Calsteren, P. & Hawkesworth, C. J. (1995). The evolution of the lithosphere in southern Africa: A perspective on the basic granulite xenoliths from kimberlites in South Africa. *Geochimica et Cosmochimica Acta* **59**, 4905-4920.
Ireland, T. R., Rudnick, R. L. & Spetsius, Z. (1994). Trace elements in diamond inclusions from eclogites reveal link to Archean granites. *Earth and Planetary Science Letters* **128**, 199-213.
Jacob, D., Jagoutz, E., Lowry, D., Mattey, D. & Kudrjavtseva, G. (1994). Diamondiferous eclogites from Siberia: remnants of Archean oceanic crust. *Geochimica et Cosmoschimica Acta* **58**, 5191-5207.
Jacob, D. E. (2004). Nature and origin of eclogite xenoliths from kimberlites. *Lithos* **77**, 295-316.
Jacob, D. E., Bizimis, M. & Salters, V. J. M. (2005). Lu-Hf and geochemical systematics of recycled ancient oceanic crust: evidence from Roberts Victor eclogites. *Contributions to Mineralogy and Petrology* **148**, 707-720.
Jones, M. Q. W. (1987). Heat-flow and heat-production in the Namaqua Mobile Belt, South-Africa. *Journal of Geophysical Research-Solid Earth and Planets* **92**, 6273-6289.
Kennedy, C. S. & Kennedy, G. C. (1976). The equilibrium boundary between graphite and diamond *Journal of Geophysical Research* **81**, 2467-2470.
Kopylova, M. G., Beausoleil, Y., Goncharov, A., Burgess, J. & Strand, P. (2016). Spatial distribution of eclogite in the Slave cratonic mantle: The role of subduction. *Tectonophysics* **672**, 87-103.
Krogh, E. J. (1988). The garnet-clinopyroxene Fe-Mg geothermometer: a reinterpretation of experimental data. *Contributions to Mineralogy and Petrology* **99**, 44-48.
Krogh Ravna, E. (2000). The garnet–clinopyroxene Fe2+–Mg geothermometer: an updated calibration. *Journal Metamorphic Geology* **18**, 211-219.
Krogh Ravna, E. & Terry, M. P. (2004). Geothermobarometry of UHP and HP eclogites and schists – an evaluation of equilibria among garnet–clinopyroxene– kyanite–phengite–coesite/quartz. *Journal of Metamorphic Geology* **22**, 579-592.
le Roex, A. & Class, C. (2016). Metasomatic enrichment of Proterozoic mantle south of the Kaapvaal Craton, South Africa: origin of sinusoidal REE patterns in clinopyroxene and garnet. *Contributions to Mineralogy and Petrology* **171**, 14: https://doi.org/10.1007/s00410-00015-01222-00418.
le Roux, P. J., le Roex, A. P., Schilling, J.-G., Shimizu, N., Perkins, W. W. & Pearce, N. J. G. (2002). Mantle heterogeneity beneath the southern Mid-Atlantic Ridge: trace element evidence for contamination of ambient asthenospheric mantle. *Earth and Planetary Science Letters* **203**, 479-498.

Levander, A., Niu, F., Lee, C. A. & Cheng, X. (2006). Imag(in)ing the continental lithosphere. *Tectonophysics* **416**, 167-185.
Long, D. J. (2005). The geothermobarometry of lower crustal xenoliths from the Goedehoop kimberlite, South Africa. *Geological Sciences*: BSc (Honours), University of Cape Town, 54.
Longerich, H. P., Jackson, S. E. & Günther, D. (1996). Laser Ablation Inductively Coupled Plasma Mass Spectrometric Transient Signal Data Acquisition and Analyte Concentration Calculation. *Journal of Analytical Atomic Spectrometry* **11**, 899-904.
MacGregor, I. D. & Carter, J. L. (1970). The chemistry of clinopyroxenes and garnets of eclogite and peridotite xenoliths from the Roberts Victor Mine, South Africa. *Physics of Earth and Planetary Interiors* **3**, 391-397.
McCandless, T. E. & Gurney, J. J. (1989). Sodium in garnet and potassium in Clinopyroxene: criteria for classifying mantle eclogites. *Kimberlites and related rocks. Vol.2. Their mantle-crust setting, diamonds and diamond exploration*: Geological Society of Australia Special Publication, 827-832.
Mengel, K. & Kern, H. (1992). Evolution of the petrological and seismic Moho - implications for the continental-crust mantle boundary. *Terra Nova* **4**, 109-116.
Nguuri, T. K., Gore, J., James, D. E., Webb, S. J., Wright, C., Zengeni, T. G., Gwavava, O. & Snoke, A. (2001). Crustal structure beneath southern Africa and its implications for the formation and evolution of the Kaapvaal and Zimbabwe cratons. *Geophysical Research Letters* **28**, 2501-2504.
Norman, M. D., Pearson, N. J., Sharma, A. & Griffin, W. L. (1996). Quantitative analysis of trace elements in geological materials by laser ablation ICPMS: Instrumental operating conditions and calibration values of NIST glasses. *Geostandards Newsletter* **20**, 247-261.
Pearce, N. J. G., Perkins, W. T., Westgate, J. A., Gorton, M. P., Jackson, S. E., Neal, C. R. & Chenery, S. P. (1997). A Compilation of New and Published Major and Trace Element Data for NIST SRM 610 and NIST SRM 612 Glass Reference Materials. *Journal of Geostandards and Geoanalysis* **21**, 115-144.
Pearson, N. J., O'Reilly, S. Y. & Griffin, W. L. (1991). Heterogeneity in the thermal state of the lower crust and upper mantle beneath eastern Australia. *Exploration Geophysics* **22**, 295-298.
Pearson, N. J., Oreilly, S. Y. & Griffin, W. L. (1995). The crust-mantle boundary beneath cratons and craton margins: A transect across the south-west margin of the Kaapvaal craton. *Lithos* **36**, 257-287.
Pollack, H. N. & Chapman, D. S. (1977). On the regional variation of heat flow, geotherms and lithospheric thickness. *Tectonophysics* **38**, 279-296.
Pouchou, J. L. & Pichoir, F. (1984). A new model for quantitative X-ray microanalysis. Part I: application to the analysis of homogeneous samples. *Research Aerospace* **3**, 167-192.
Powell, R., Holland, T. & Worley, B. (1998). Calculating phase diagrams involving solid solutions via non-linear equations, with examples using THERMOCALC. *Journal of Metamorphic Geology* **16**, 577-588.
Proyer, A., Dachs, E. & McCammon, C. (2004). Pitfalls in geothermobarometry of eclogites: Fe3+ and changes in the mineral chemistry of omphacite at ultrahigh pressures. *Contributions to Mineralogy and Petrology* **147**, 305-318.
Rehfeldt, T., Jacob, D. E., Carlson, R. W. & Lowry, D. (2008). Contrasting types of metasomatism in dunite, wehrlite and websterite xenoliths from Kimberley, South Africa. *Geochimica et Cosmochimica Acta* **72**, 5722-5756.
Robey, J. (1981). Kimberlites in the Central Cape Province, R.S.A.: University of Cape Town.
Rollinson, H. (1997). Eclogite xenoliths in west Afrian kimberlites as residues of Archaean granitoid crust formation. *Nature* **389**, 173-176.

Schmitz, M. D. & Bowring, S. A. (2000). The significance of U–Pb zircon dates in lower crustal xenoliths from the southwestern margin of the Kaapvaal craton, southern Africa. *Chemical Geology* **172**, 56-76.
Schmitz, M. D. & Bowring, S. A. (2004). Lower crustal granulite formation during Mesoproterozoic Namaqua-Natal collisional orogenesis, southern Africa. *South African Journal of Geology* **107**, 261-284.
Shee, S. R. (1978). The mineral chemistry of xenoliths from the Orapa kimberlite pipe, Botswana. Unpublished: Cape Town.
Shirey, S. B., Carlson, R. W., Richardson, S. H., Menzies, A. H., Gurney, J. J., Pearson, D. G., Harris, J. W. & Wiechert, U. (2001). Archean emplacement of eclogitic components into the lithospheric mantle during formation of the Kaapvaal craton. *Geophysical Research Letters* **28**, 2509-2512.
Shirey, S. B., Harris, J. W., Richardson, S. H., Fouch, M. J., James, D. E., Cartigny, P., Deines, P. & Viljoen, F. (2002). Diamond genesis, seismic structure, and evolution of the Kaapvaal-Zimbabwe craton. *Science* **297**, 1683-1686.
Smit, K. V., Stachel, T., Creaser, R. A., Ickert, R. B., DuFrane, S. A., Stern, R. A. & Seller, M. (2014). Origin of eclogite and pyroxenite xenoliths from the Victor kimberlite, Canada, and implications for Superior craton formation. *Geochimica et Cosmochimica Acta* **125**, 308-337.
Smith, C. B., Clark, T. C., Barton, E. S. & Bristow, J. W. (1994). Emplacement ages of kimberlite occurrences in the Prieska region, southwest border of the Kaapvaal Craton, South Africa. *Chemical Geology* **113**, 149-169.
Smyth, J. R. (1980). Cation vacancies and the crystal chemistry of breakdown reactions in kimberlitic omphacites *American Mineralogist* **65**, 1257–1264.
Snyder, G. A., Taylor, L. A., Crozaz, G., Halliday, A. N., Beard, B. L., Sobolev, V. N. & Sobolev, N. V. (1997). The origins of Yakutian eclogite xenoliths. *Journal of Petrology* **38**, 85-113.
Sun, C. & Liang, Y. (2015). A REE-in-garnet–clinopyroxene thermobarometer for eclogites, granulites and garnet peridotites. *Chemical Geology* **393-394**, 79-92.
Sun, S.-s. & McDonough, W. F. (1989). Chemical and isotopic systematics of oceanic basalts: implications for mantle composition and processes. In: Saunders, A. D. & Norry, M. J. (eds.) *Magmatism in the Ocean Basins*: Geological Society, 313-345.
Tanaka, T., Togashi, S., Kamioka, H., Amakawa, H., Kagami, H., Hamamoto, T., Yuhara, M., Orihashi, Y., Yoneda, S., Shimizu, H., Kunimaru, T., Takahashi, K., Yanagi, T., Nakano, T., Fujimaki, H., Shinjo, R., Asahara, Y., Tanimizu, M. & Dragusanu, C. (2000). JNdi-1: a neodymium isotopic reference in consistency with LaJolla neodymium. *Chemical Geology* **168**, 279-281.
Taylor, L. A. & Neal, C. R. (1989). Eclogites with oceanic crustal and mantle signatures from the Bellsbank kimberlite, South Africa, Part 1: mineralogy, petrography, and whole-rock chemistry. *Journal of Geology* **97**, 551-567.
Taylor, L. A., Snyder, G. A., Keller, R., Remley, D. A., Anand, M., Wiesli, R., Valley, J. & Sobolev, N. V. (2003). Petrogenesis of group A eclogites and websterites: evidence from the Obnazhennaya kimberlite, Yakutia. *Contributions to Mineralogy and Petrology* **145**, 424-443.
Taylor, W. R. (1998). An experimental test of some geothermometer and geobarometer formulations for upper mantle peridotites with application to the thermobarometry of fertile lherzolite and garnet websterite. *Neues Jahrbuch Fur Mineralogie-Abhandlungen* **172**, 381-408.
Tinguely, C. E., Gregoire, M. & le Roex, A. P. (2008). Eclogite and pyroxenite xenoliths from off-craton kimberlites near the Kaapvaal Craton, South Africa. *Comptes Rendus Geoscience* **340**, 811-821.
Viljoen, K. S. (1995). Graphite- and diamond-bearing eclogite xenoliths from the Bellsbank kimberlites, northern Cape, South Africa. *Contribributions to Mineralogy and Petrology* **121**, 414-423.

Viljoen, K. S., Schulze, D. J. & Quadling, A. G. (2005). Contrasting group I and group II eclogite xenolith petrogenesis: petrological, trace element and isotopic evidence from eclogite, garnet-websterite and alkremite xenoliths in the Kaalvallei kimberlite, South Africa. *Journal of Petrology* **46**, 2059-2090.
Viljoen, K. S., Smith, C. B. & Sharp, Z. D. (1996). Stable and radiogenic isotope study of eclogite xenoliths from the Orapa kimberlite, Botswana. *Chemical Geology* **131**, 235-255.

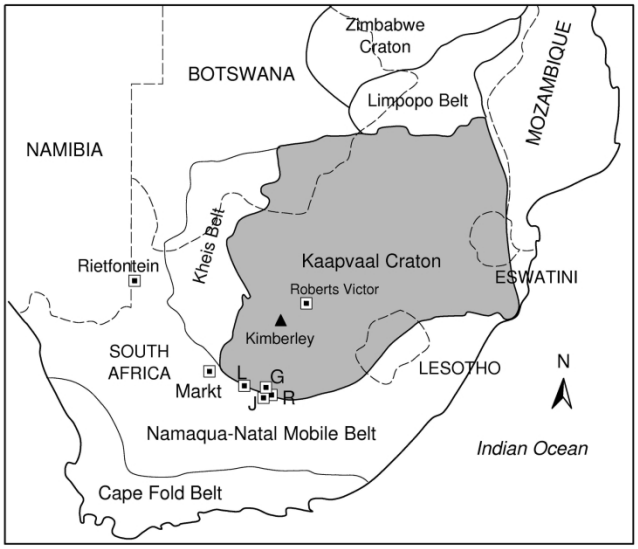

Fig. 1

Figure 1: Map showing the location of Jachtfontein (J), Lovedale (L), Markt, Roodekraal (R) and Goedehoop (G) kimberlites relative to the Kaapvaal craton and Namaqua-Natal Belt. The on-craton eclogite locality of Roberts Victor and the off-craton Rietfontein locality are also shown.

203x266mm (300 x 300 DPI)

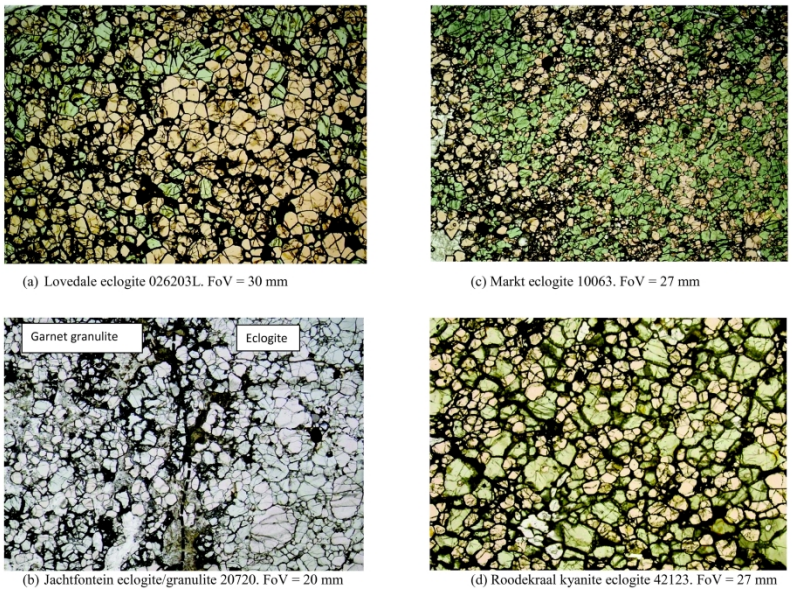

Fig. 2

Figure 2: Selected photomicrographs showing salient features of selected eclogite xenoliths. (a) Eclogite 026203L from Lovedale, (b) Eclogite 20720 from Jachtfontein showing contact between eclogite (20720e) on the right and garnet granulite (20720g) on the left, (c) Eclogite 10063 from Markt, (d) Kyanite eclogite 42123 from Roodekraal.

296x209mm (300 x 300 DPI)

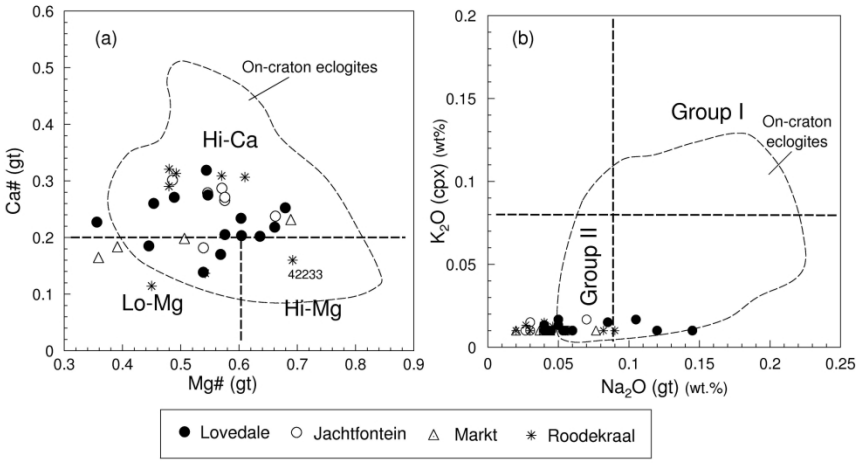

Fig. 3

Figure 3: (a) Ca# (atomic Ca/Ca+Fe+Mn+Mg) versus Mg# (atomic Mg/Mg+Fe) in garnets from craton margin eclogites. Classification boundaries from Aulbach et al. (2017). Field for on-craton eclogites includes data from Roberts Victor (Hatton, 1978), Jagersfontein and Jwaneng (this study), Lace (Aulbach & Viljoen, 2015), Orapa (Shee, 1978), Kaalvallei (Viljoen et al., 2005). (b) K2O (wt.%) in clinopyroxene versus Na2O (wt.%) in garnet for craton margin eclogites showing Group I and Group II boundaries from McCandless and Gurney (1989). Field for on-craton eclogites as for (a).

203x266mm (300 x 300 DPI)

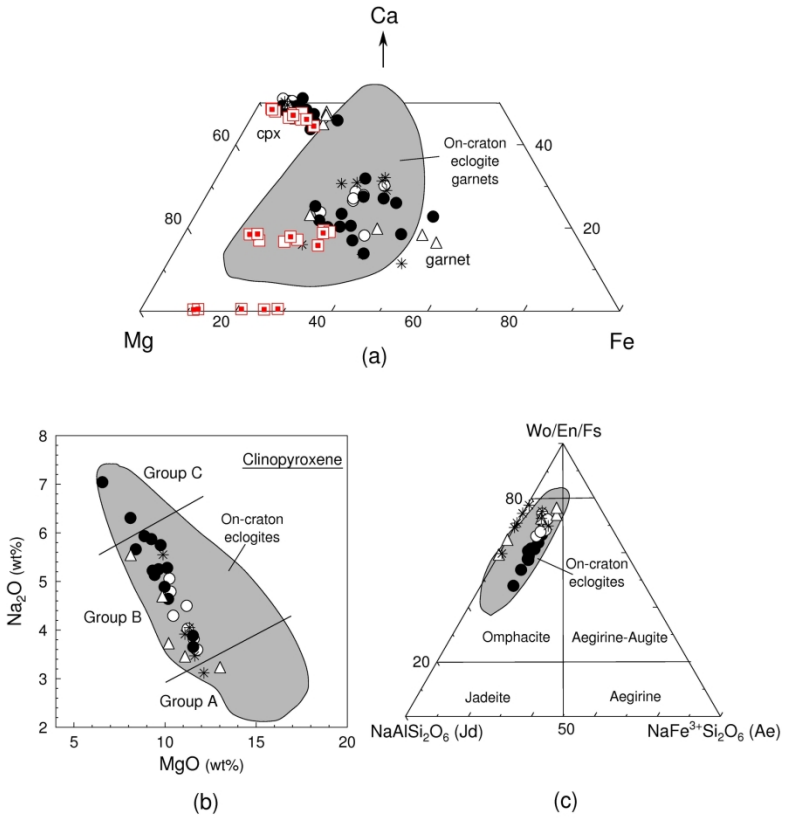

Fig. 4

Figure 4: (a) Ca-Mg-Fe compositional variation of clinopyroxene and garnet in craton margin eclogites, garnet clinopyroxenites and garnet websterites. (b) Na2O–MgO (wt.%) variation in clinopyroxene from craton margin eclogites. Group A, B and C subdivisions from (Taylor & Neal, 1989). (c) Compositional variation of craton margin eclogites with respect to Diopside-Jadeite-Aegirine. Ferric iron calculated following Droop (1987). Field for on-craton eclogites as for Fig. 3. Symbols for eclogites in all three panels as for Fig. 3; garnet clinopyroxenites: red open squares; garnet websterites: red open squares with solid centre.

203x266mm (300 x 300 DPI)

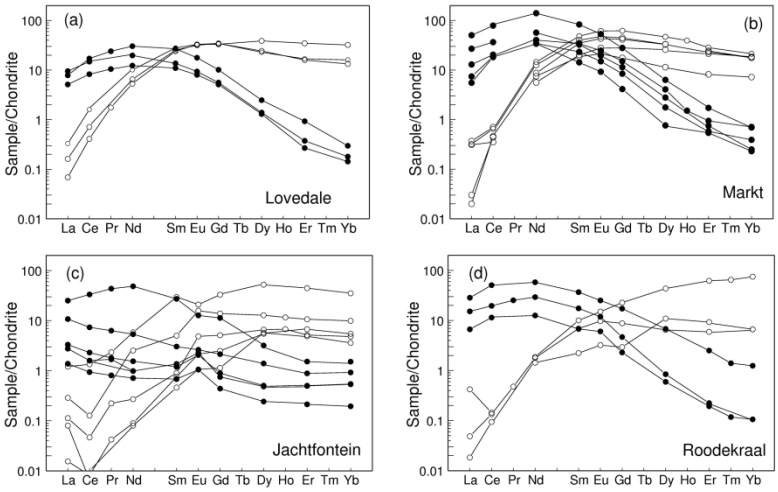

Fig. 5

Figure 5: Chondrite normalised REE diagrams for clinopyroxene (solid circles) and garnet (open circles) in representative craton margin eclogites from Lovedale (a), Markt (b), Jachtfontein (c) and Roodekraal (d). Chondrite normalising values from (Sun & McDonough, 1989).

297x209mm (300 x 300 DPI)

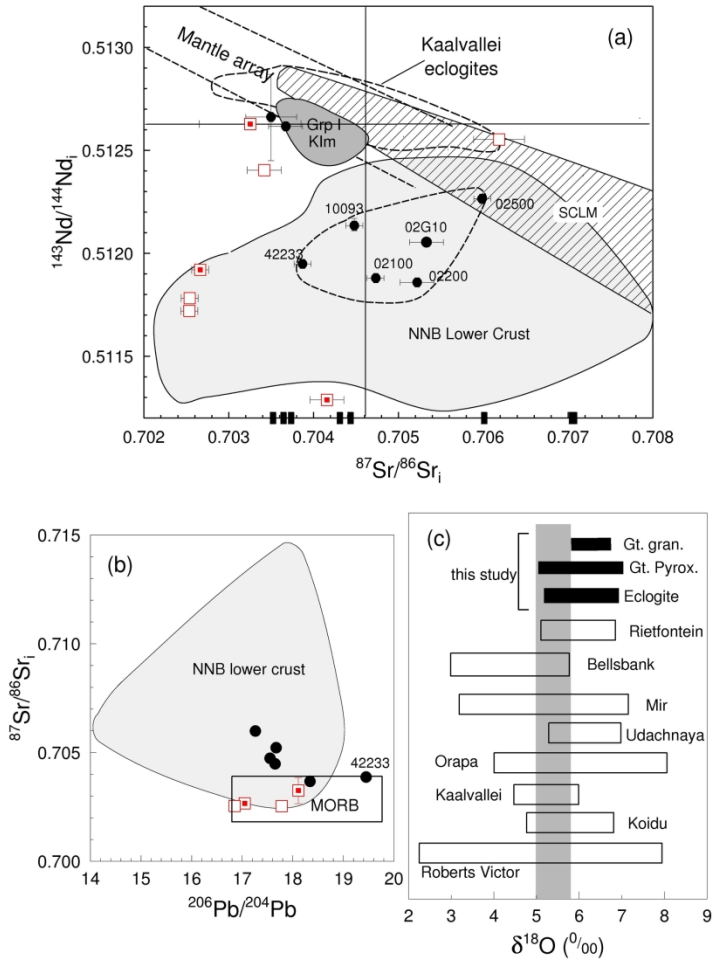

Fig. 6

Figure 6: (a) Initial 143Nd/144Nd versus 87Sr/86Sr isotope ratios measured in clinopyroxene from craton margin eclogites and garnet pyroxenites. Symbols as in Figure 4. Where Nd isotope data are not available (for laser ablation determined 87Sr/86Sr) data have been plotted on the x-axis at 143Nd/144Nd = 0.5112 to show range in 87Sr/86Sr. Initial ratios calculated for age of kimberlite pipe. Two sigma error bars are shown or are less than symbol size. Field for off-craton Group I kimberlites from Becker and le Roex (2006). Field for Namaqua-Natal Belt (NNB) lower crust from Class and le Roex (2011), Huang et al. (1995) and this study. Field for clinopyroxenes from Kaalvallei eclogites from Viljoen et al. (2005). (b) Initial 87Sr/86Sr versus 206Pb/204Pb measured in clinopyroxene from craton margin eclogites and garnet pyroxenites. Two sigma error bars are shown, or are less than symbol size. MORB field shown schematically. Field for Namaqua-Natal Belt (NNB) lower crust from Class and le Roex (2011), Huang et al. (1995) and this study. (c) Oxygen isotope ratios (in ‰) in craton margin eclogites, garnet pyroxenites and garnet granulites. δ18O data for other eclogite localities from Jacob (2004 and references therein).

203x266mm (300 x 300 DPI)

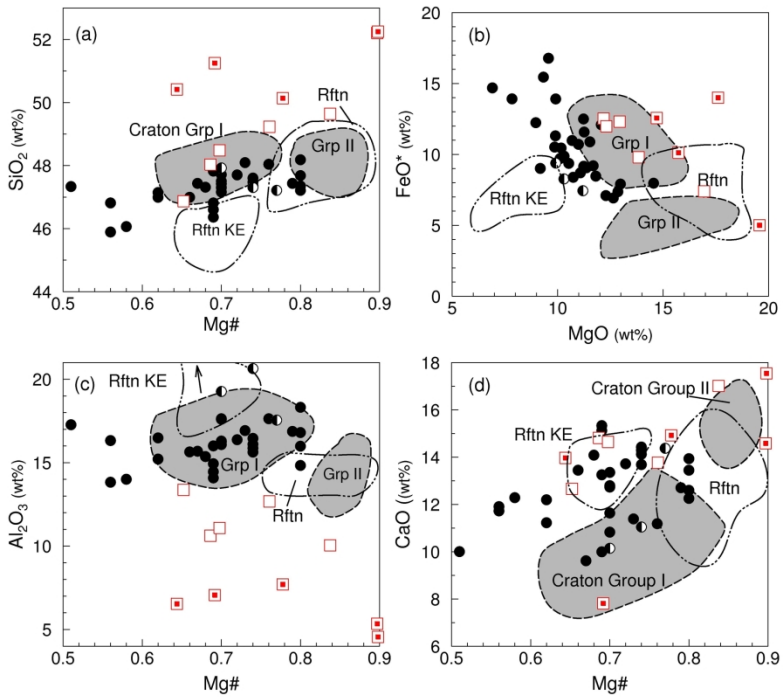

Fig. 7

Figure 7: Variations in selected major elements from reconstructed bulk rock compositions for craton margin eclogites and garnet pyroxenites. Symbols as in Figure 4. The few kyanite eclogites are shown with half-filled circles. Field for off-craton Rietfontein eclogites (Rftn) and Rietfontein kyanite eclogites (Rftn KE) from Appleyard et al. (2007). Fields for Group I and Group II on-craton eclogites in grey from Viljoen et al., (2005), Aulbach and Viljoen (2015), Hatton (1978), Shee (1978), this study.

203x266mm (300 x 300 DPI)

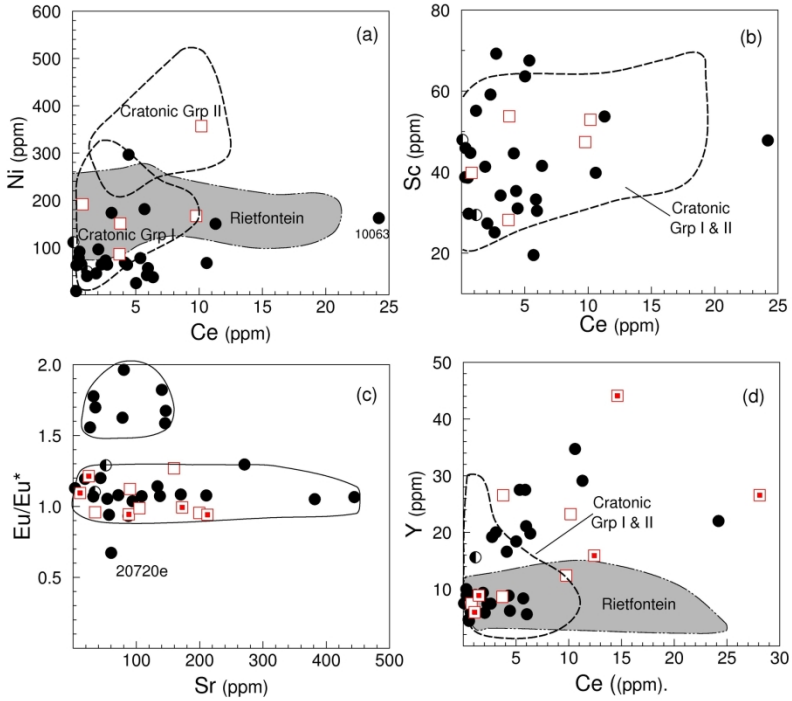

Fig. 8

Figure 8: Variation in selected trace elements from reconstructed bulk rock compositions for craton margin eclogites and garnet pyroxenites. Symbols as in Figure 4. Eu*= chondrite normalised Eu/(Sm1/2*Gd1/2). Field for off-craton Rietfontein eclogites from Appleyard et al. (2007). Fields for Group I and Group II on-craton eclogites from Viljoen et al. (2005), Aulbach and Viljoen (2015), Hatton (1978), Shee (1978) and this study.

203x266mm (300 x 300 DPI)

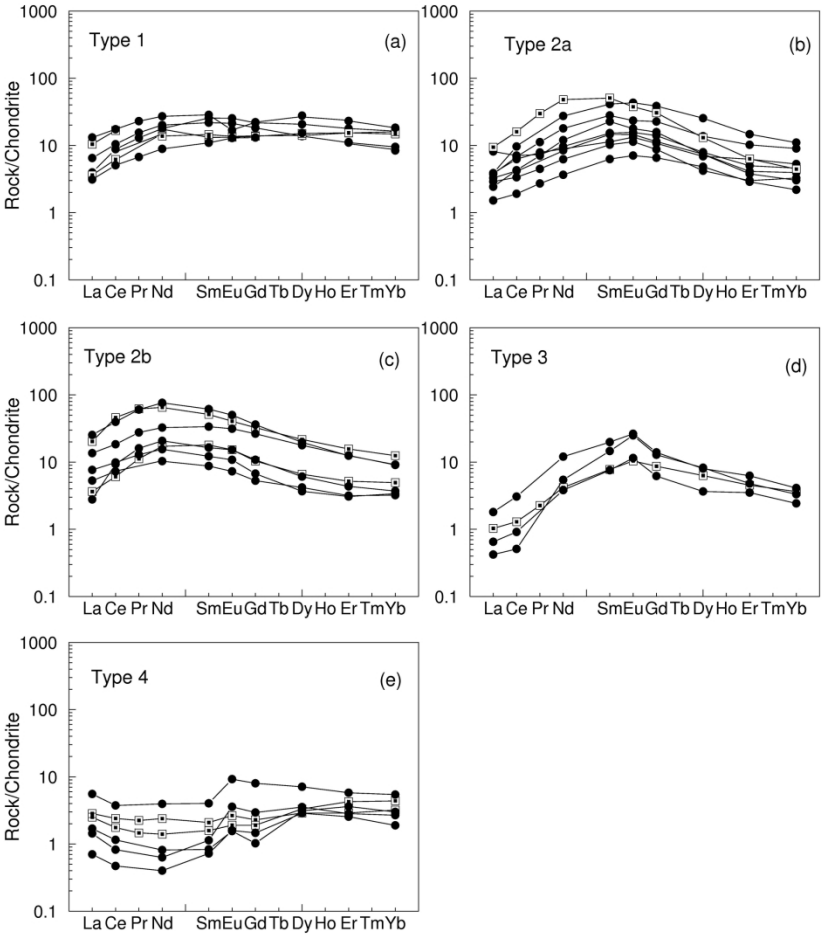

Fig. 9

Figure 9: Chondrite normalised REE patterns in reconstructed bulk rock compositions of eclogites and some garnet pyroxenites. Samples have been subdivided into four types with distinctive patterns. See text for further discussion. Chondrite normalising values from Sun and McDonough (1989). Solid symbols: eclogites; open symbols: garnet pyroxenites.

203x266mm (300 x 300 DPI)

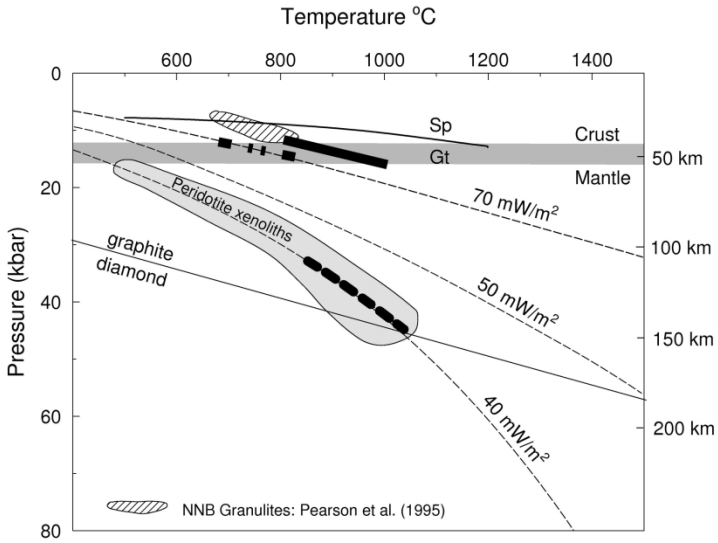

Fig. 10

Figure 10: P-T diagram showing calculated equilibrium temperatures for the craton margin eclogites plotted against the 40 mW.m-2 geotherm (Pollack & Chapman, 1977) – dashed black line, and parallel to the geotherm slope using an average of 1.5 GPa pressure – solid black line, using Ellis and Green (1979). Calculated equilibrium temperatures for garnet pyroxenites (assuming 1.5 GPa pressure) lie along the 70 mW.m-2 geotherm (short and long dashes). Also shown is the field of calculated equilibrium pressures and temperatures for peridotite xenoliths from craton margin kimberlites (le Roex & Class, 2016) and the P-T field for garnet granulites from the Namaqua-Natal Belt (Pearson et al., 1995). Graphite-diamond boundary from (Kennedy & Kennedy, 1976).

203x266mm (300 x 300 DPI)

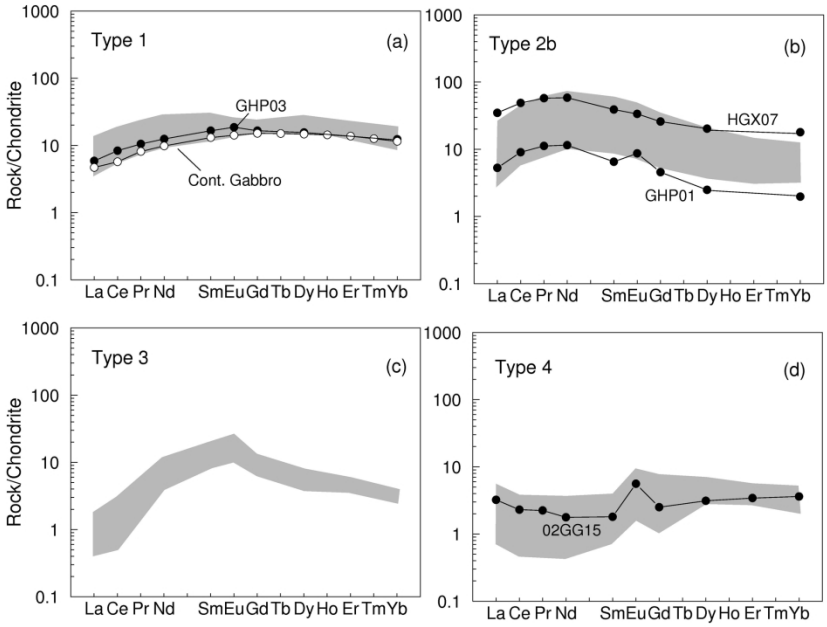

Fig. 11

Figure 11: Fields highlighting the four different chondrite normalised REE patterns recognised amongst reconstructed bulk rock compositions of craton margin eclogites and garnet pyroxenites with superimposed REE patterns from selected garnet granulite xenoliths from this study. Reconstructed bulk rock compositions of the garnet granulite xenoliths calculated using modal abundances in analysed samples. (a) Type 1 REE patterns with superimposed pattern of garnet granulite GHP03 and an example of a continental gabbro without Eu anomaly. (b) Type 2b REE pattern with superimposed REE patterns of garnet granulites HGX07 and GHP01. (c) Field of Type 3 REE patterns. (d) Type 4 REE pattern with superimposed REE pattern of garnet granulite 02GG15. Chondrite normalising values from Sun and McDonough (1989).

203x266mm (300 x 300 DPI)

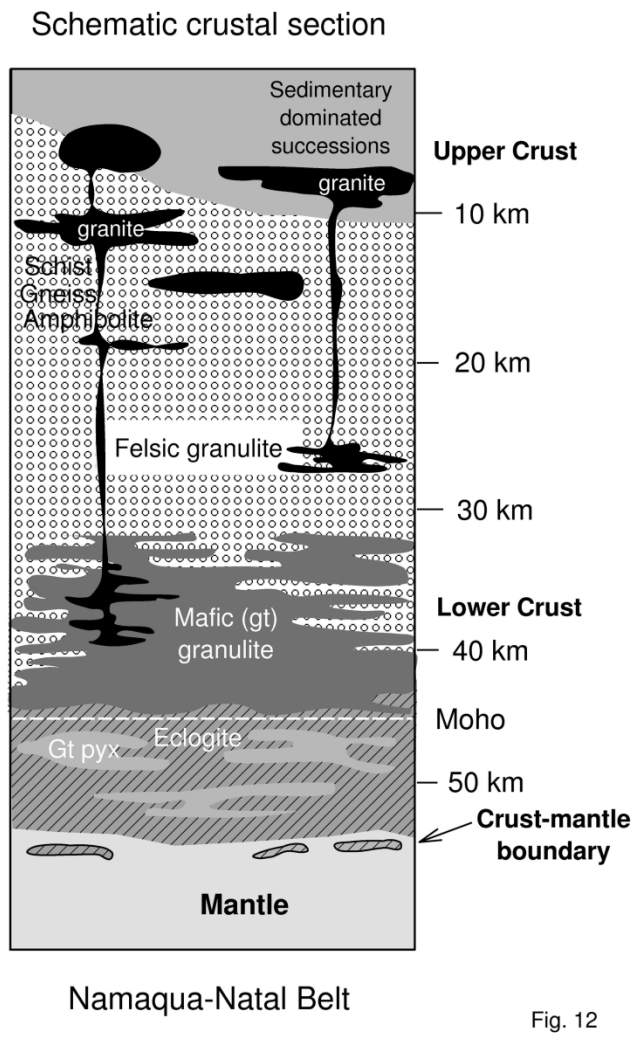

Figure 12: Schematic cross-section of the Namaqua-Natal Belt crust beneath the region of study, showing eclogite and garnet pyroxenite lithologies extending below the seismic Moho. Modified from Hawkesworth and Kemp (2006).

203x266mm (300 x 300 DPI)